

1 **A Comparative Study of Two-way and**
2 **Offline Coupled WRF v3.4 and CMAQ v5.0.2**
3 **over the Contiguous U.S.: Performance**
4 **Evaluation and Impacts of Chemistry-**
5 **Meteorology Feedbacks on Air Quality**

6 Kai Wang¹, Yang Zhang^{1*}, Shaocai Yu^{2*}, David C. Wong³, Jonathan Pleim³, Rohit Mathur³,
7 James T. Kelly⁴, and Michelle Bell⁵

8 ¹Department of Civil and Environmental Engineering, Northeastern University, Boston, MA
9 02115

10 ²Key Laboratory of Environmental Remediation and Ecological Health, Ministry of Education;
11 Research Center for Air Pollution and Health, College of Environment and Resource Sciences,
12 Zhejiang University, Hangzhou, Zhejiang 310058, P.R. China

13 ³Center for Environmental
14 Measurement and Modeling, U.S. EPA, RTP, NC 27711

15 ⁴Office of Air Quality Planning and Standards, U.S. EPA, RTP, NC 27711

16 ⁵School of Forestry & Environmental Studies, Yale University, New Haven, CT 06511

17

18 **Correspondence to:* Yang Zhang (ya.zhang@northeastern.edu); Shaocai Yu (shaocaiyu@zju.edu.cn)

19

20 **Abstract**

21 The two-way coupled Weather Research and Forecasting and Community Multiscale Air
22 Quality (WRF-CMAQ) model has been developed to more realistically represent the atmosphere
23 by accounting for complex chemistry-meteorology feedbacks. In this study, we present a
24 comparative analysis of two-way (with consideration of both aerosol direct and indirect effects)
25 and offline coupled WRF v3.4 and CMAQ v5.0.2 over the contiguous U.S. Long-term (five-year
26 of 2008-2012) simulations using WRF-CMAQ with both offline and two-way coupling modes
27 are carried out with anthropogenic emissions based on multiple years of the U.S. National
28 Emission Inventory and chemical initial and boundary conditions derived from an advanced
29 Earth system model (i.e., a modified version of the Community Earth System Model/Community
30 Atmospheric Model). The comprehensive model evaluations show that both two-way WRF-
31 CMAQ and WRF-only simulations perform well for major meteorological variables such as
32 temperature at 2 m, relative humidity at 2 m, wind speed at 10 m, and precipitation (except for
33 against the National Climatic Data Center data) as well as shortwave/longwave radiation. Both
34 two-way and offline CMAQ also show good performance for ozone (O₃) and fine particulate
35 matter (PM_{2.5}). Due to the consideration of aerosol direct and indirect effects, two-way WRF-
36 CMAQ shows improved performance over offline-coupled WRF and CMAQ in terms of
37 spatiotemporal distributions and statistics, especially for radiation, cloud forcing, O₃, sulfate,
38 nitrate, ammonium, and elemental carbon as well as tropospheric O₃ residual and column
39 nitrogen dioxide (NO₂). For example, the mean biases have been reduced by more than 10 W m⁻²
40 for shortwave radiation and cloud radiative forcing and by more than 2 ppb for max 8-h O₃.
41 However, relatively large biases still exist for cloud predictions, some PM_{2.5} species, and PM₁₀,
42 which warrant follow-up studies to better understand those issues. The impacts of chemistry-

43 meteorological feedbacks are found to play important roles in affecting regional air quality in the
44 U.S. by reducing domain-average concentrations of carbon monoxide (CO), O₃, nitrogen oxide
45 (NO_x), volatile organic compounds (VOCs), and PM_{2.5} by 3.1% (up to 27.8%), 4.2% (up to
46 16.2%), 6.6% (up to 50.9%), 5.8% (up to 46.6%), and 8.6% (up to 49.1%), respectively, mainly
47 due to reduced radiation, temperature, and wind speed. The overall performance of the two-way
48 coupled WRF-CMAQ model achieved in this work is generally good or satisfactory and the
49 improved performance for two-way coupled WRF-CMAQ should be considered along with other
50 factors in developing future model applications to inform policy making.

51 **Keywords:** CMAQ, Two-way coupling, Evaluation, Chemistry-meteorology feedback

52 **1. Introduction**

53 The Community Multiscale Air Quality (CMAQ) modeling system developed by the U.S.
54 Environmental Protection Agency (EPA) (Byun and Schere, 2006; Scheffe et al., 2016; San
55 Joaquin Valley APCD, 2018; Pye et al., 2020; U.S. EPA, 2020) has been extensively used by
56 both scientific community and governmental agencies over various geographical regions and
57 under different meteorological and air pollution conditions to address major key air quality
58 issues such as atmospheric ozone (O₃), acid rain, regional haze, and trans-boundary or long-
59 range transport of air pollutants during the past decades over North America (Zhang et al.,
60 2009a,b; Wang and Zhang, 2012; Hogrefe et al., 2015), Asia (Wang et al., 2009, 2012; Liu et al.,
61 2010; Zheng et al., 2015; Li et al., 2017; Xing et al., 2017; Yu et al., 2018; Mehmood et al.,
62 2020), and Europe (Kukkonen et al., 2012; Mathur et al., 2017; Solazzo et al., 2017). The
63 CMAQ model is traditionally driven offline by the three-dimensional meteorology fields
64 generated separately from other meteorological models such as the Weather Research and
65 Forecasting (WRF) model, and the dynamic feedbacks of chemistry predictions on meteorology

66 are neglected. However, more recently (IPCC, 2018), chemistry-meteorology feedbacks have
67 been found to play important roles in affecting the both global and regional climate change and
68 air quality (Jacobson et al., 1996; Mathur et al., 1998; Ghan et al., 2001; Zhang, 2008; Zhang et
69 al., 2010, 2015a,b, 2017; Grell and Baklanov, 2011; Wong et al., 2012; Baklanov et al., 2014; Yu
70 et al., 2014; Gan et al., 2015a; Wang et al., 2015a; Xing et al., 2015a,b; Yahya et al., 2015a,b;
71 Hong et al., 2017; Jung et al., 2019). Feedbacks of aerosols on radiative transfer through aerosol-
72 radiation interactions (i.e., aerosol direct forcing) and aerosol-cloud interactions (i.e., aerosol
73 indirect forcing) are especially important (Zhang, 2008; Zhang et al., 2015a,b; Baklanov et al.,
74 2014; Wang et al., 2015a; Yahya et al., 2015a,b). Recognizing this importance, as well as the
75 recent advances in knowledge on chemistry-meteorology interactions and computational
76 resources, the U.S. EPA developed a two-way coupled WRF-CMAQ model that accounts for the
77 aerosol direct effect alone (Wong et al., 2012). This version of CMAQ has been applied for both
78 regional and hemispheric studies (Wang et al., 2014; Hogrefe et al., 2015; Xing et al., 2016,
79 2017; Hong et al., 2017, 2020; Sekiguchi et al., 2018; Yoo et al., 2019). For example, Xing et al.
80 (2016) showed that aerosol direct feedbacks may further improve air quality resulting from
81 emission controls in the U.S. and also indicated that coupled models are key tools for quantifying
82 such feedbacks. Reduction in atmospheric ventilation resulting from aerosol induced surface
83 cooling can exacerbate ground level air pollution. Hong et al. (2017) estimated an increase by
84 4.8%-9.5% in concentrations of major air pollutants over China in winter due to incorporation of
85 such effects. Xing et al. (2017) reported that the aerosol direct effects could reduce daily max 1h
86 O₃ by up to 39 μg m⁻³ over China in January through reducing solar radiation and photolysis
87 rates. Hong et al. (2020) found that the benefits of reduced pollutant emissions through
88 weakening aerosol direct effects can largely offset the additional deaths caused by the warming

89 effect of greenhouse gases over China. Some of those studies have also found that the missing
90 aerosol indirect effects in WRF-CMAQ may introduce large model biases on their simulations of
91 radiation and thus air quality (Wang et al., 2014; Sekiguchi et al., 2018; Yoo et al., 2019). There
92 has been a growing awareness that both aerosol effects should be considered together to provide
93 greater fidelity in coupling complex atmospheric processes among chemistry, aerosols, cloud,
94 radiation, and precipitation (Grell and Baklanov, 2011). To address this issue and better represent
95 the one-atmosphere modeling capability of CMAQ, Yu et al. (2014) further extended the two-
96 way coupled WRF-CMAQ model by including aerosol indirect effects and improved WRF-
97 CMAQ's capability for predicting cloud and radiation variables.

98 Different from the traditional online integrated air quality models such as the Gas,
99 Aerosol, Transport, Radiation, General Circulation, and Mesoscale Meteorological (GATOR-
100 GCMM) model (Jacobson, 2001), the WRF model coupled with chemistry (WRF/Chem; Grell et
101 al., 2005) and the WRF model coupled with the Community Atmosphere Model version 5
102 (WRF-CAM5; Ma et al., 2013; Zhang et al., 2015a,b; 2017), in which atmospheric dynamics and
103 chemistry are integrated and simulated altogether without an interface between meteorology and
104 atmospheric chemistry (Zhang et al., 2013), two-way WRF-CMAQ (also referred to as the online
105 access model) is created by combining existing meteorology (i.e., WRF) and atmospheric
106 chemistry (i.e., CMAQ) models with an interactive interface (Yu et al., 2014). As pointed out by
107 Yu et al. (2014), the main advantage of two-way CMAQ is to allow the existing numerical
108 techniques to be used in both WRF and CMAQ to facilitate future independent development of
109 both models while also maintaining CMAQ as a stand-alone model (the offline capability). In the
110 past, a number of studies have compared and evaluated online vs. offline-coupled model
111 performance (Pleim et al, 2008; Matsui et al., 2009; Wilczak et al., 2009; Lin et al., 2010;

112 Herwehe et al., 2011; Yu et al., 2011; Wong et al., 2012; Zhang et al., 2013, 2016a; Choi et al.,
113 2019). However due to the missing offline-coupled mode or component for most online-coupled
114 models, many of those intercomparison studies are subject to some key limitations such as
115 inconsistent model treatments in chemical options (Matsui et al., 2009; Lin et al., 2010; Zhang et
116 al., 2013; Choi et al., 2019) or in both physical and chemical options (Wilczak et al., 2009;
117 Herwehe et al., 2011; Zhang et al., 2016a), different domain projection methods or resolutions
118 (Wilczak et al., 2009; Lin et al., 2010; Zhang et al., 2013), or disunified model inputs (Wilczak et
119 al., 2009; Lin et al., 2010; Zhang et al., 2013). Due to the unique coupling approach, two-way
120 WRF-CMAQ can be used to overcome those limitations and set up ideal intercomparisons
121 between online and offline simulations using consistent model treatments (Pleim et al, 2008; Yu
122 et al., 2011; Wong et al., 2012).

123 In this study, we provide a robust examination of model improvements by considering
124 chemistry-meteorology feedbacks and their impacts on the U.S. air quality using the two-way
125 WRF-CMAQ model (same version as in Yu et al., 2014) with both aerosol direct and indirect
126 effects. Long-term (five-year of 2008-2012) simulations using both two-way and offline coupled
127 WRF and CMAQ models are carried out and compared to the best of our knowledge for the first
128 time over the contiguous U.S. (CONUS) with anthropogenic emissions based on multiple years
129 of the U.S. National Emission Inventory (NEI) and chemical initial and boundary conditions
130 (ICONS/BCONS) downscaled from the advanced Earth system model, i.e., an updated version of
131 the Community Earth System Model/CAM5 (CESM/CAM5; He and Zhang, 2014; Glotfelty et
132 al., 2017). Our objectives include 1) perform a comprehensive model evaluation for major
133 meteorological variables and chemical species from this long-term application of the two-way

134 coupled WRF-CMAQ; and 2) conduct a comparative study of two-way and offline coupled WRF
135 and CMAQ to examine the impacts of chemistry-meteorology interactions on U.S. air quality.

136 Compared to previous studies in the literature, there are a few key features of this work.
137 First, the intercomparisons between two-way (or online) and offline WRF-CMAQ are performed
138 here using consistent model configurations including both physical/chemical options and inputs.
139 Second, unlike a few previous intercomparison studies (Pleim et al, 2008; Yu et al., 2011; Wong
140 et al., 2012) using two-way WRF-CMAQ with only aerosol direct effects for relatively short
141 episodes, the model version in this work includes both aerosol direct and indirect effects and
142 simulations are conducted for multiple years to provide more robust assessments. Third,
143 compared to other studies (e.g., Yahya et al., 2015a,b; Choi et al., 2019) focusing on the impacts
144 of chemistry-meteorology feedbacks on meteorology only or limited chemical species, this study
145 performs comprehensive and extensive evaluation and comparison to demonstrate importance of
146 chemistry-meteorology feedbacks on regional meteorology and air quality.

147 **2. Model description, simulation setup, and evaluation protocols**

148 Two sets of five-year (i.e., 2008-2012) long-term simulations are conducted using the two-
149 way coupled WRF v3.4-CMAQ v5.0.2 model with both aerosol direct and indirect effects and
150 the sequentially offline-coupled WRF v3.4 and CMAQ v5.0.2 model, respectively, over the
151 CONUS with 36-km horizontal grid spacing. The vertical resolution for these simulations
152 consists of 34 layers from the surface (~38 m) to 100 hPa (~15 km). The two-way coupled WRF-
153 CMAQ includes estimations of aerosol optical properties based on prognostic aerosol size
154 distributions and composition. These aerosol optical properties are then used to modulate the
155 shortwave radiation budget estimated using the Rapid and accurate Radiative Transfer Model for

156 General circulation (RRTMG) radiation scheme (Iacono et al., 2008) in WRF. Additionally,
157 aerosol indirect effects, including the first (cloud albedo) and second (cloud lifetime) indirect
158 aerosol forcing and the glaciation (ice and mixed-phase cloud lifetime) indirect aerosol forcing
159 are also modeled. More details on the model development of this version of WRF-CMAQ can be
160 found in Yu et al. (2014). On the other hand, the WRF only model calculates the radiation
161 budgets by using prescribed aerosol optical properties such as aerosol optical depth, single
162 scattering albedo and asymmetry parameters and cloud formation by assuming default droplet
163 number concentration and fixed cloud effective radius, which may not be representative for the
164 large regions with complex air pollution conditions. Both the two-way and offline coupled WRF-
165 CMAQ use the same model configurations as shown in Table S1 in the supplementary material,
166 except that prognostic aerosol impacts on radiation and clouds are fully treated in two-way
167 WRF-CMAQ. The physics options include the RRTMG shortwave and longwave radiation
168 schemes, the Asymmetric Convective Model (ACM2) planetary boundary layer (PBL) scheme
169 (Pleim, 2007), the Pleim-Xiu (PX) land-surface scheme (Xiu and Pleim, 2001), the Morrison
170 two-moment microphysics scheme (Morrison et al., 2009), and version 2 of the Kain-Fritsch
171 (KF2) cumulus scheme (Kain, 2004). The chemical options include the Carbon Bond 2005
172 (CB05) chemical mechanism (Yarwood et al., 2005) with additional chloride chemistry (Sarwar
173 et al., 2008), the sixth generation CMAQ aerosol module (AERO6) (Appel et al., 2013), and
174 CMAQ's aqueous phase chemistry (AQCHEM). In addition, the time steps of dynamics and
175 radiation for two-way WRF-CMAQ are set as 1 min and 15 mins, respectively, and the call
176 frequency for CMAQ in the two-way coupled model is set to be 5 mins.

177 The meteorological ICONs/BCONs are generated from the National Centers for
178 Environmental Prediction Final Analysis (NCEP-FNL) datasets and the chemical

179 ICONs/BCONs are downscaled from a modified version of CESMv1.2.2/CAM5 (He and Zhang,
180 2014; Glotfelty et al., 2017). The chemical ICONs/BCONs generated from CESM simulations
181 consider the year-to-year variation. The CESM simulations have been comprehensively
182 evaluated against surface, remote sensing including satellite data, and reanalysis data for major
183 meteorological and chemical variables over Europe, Asia, North America, and the globe. The
184 results are also compared with other existing global model results and show generally
185 satisfactory/superior performance. The anthropogenic emissions are based on two versions of
186 NEI. NEI 2008 and NEI 2011 are used to cover the 5-year period, i.e., NEI 2008 for 2008-2010
187 and NEI 2011 for 2011-2012, respectively. Biogenic emissions are calculated online using the
188 Biogenic Emissions Inventory System (BEIS) v3 (Schwede et al., 2005). The sea-salt and dust
189 emissions are also generated online by CMAQ's inline modules (Zender et al., 2003; Zhang et
190 al., 2005). Two-way coupled WRF-CMAQ simulations are reinitialized every 5 days for
191 meteorology fields only. We have conducted sensitivity simulations in the past (Wang et al.,
192 2021) and found that a 5-day reinitialization frequency is more suitable to improve the overall
193 simulation quality while preserving chemistry-meteorology feedbacks. The WRF-only
194 simulations apply the same reinitialization method to make sure any deviation between two
195 simulations are more determined by the feedback processes.

196 The model evaluation in this work mainly focuses on the long-term climatological type of
197 performance in representative seasons (i.e., winter and summer) by comparing 5-year average
198 spatially and temporally matched model predictions of major surface meteorological/radiation-
199 cloud variables and surface/column chemical species against various surface/satellite
200 observations and reanalysis data (The 5-year annual results can be found in the supplemental
201 materials). A brief inter-annual comparison between observations and two-way CMAQ

202 simulations are also performed for selected major meteorological and chemical variables to
203 examine the model's capability in reproducing the year-to-year variations of those variables. The
204 surface meteorological data include temperature at 2 m (T2), relative humidity at 2 m (RH2),
205 wind speed at 10 m (WS10), and wind direction at 10 m (WD10) from the National Climatic
206 Data Center (NCDC), and precipitation from the NCDC, the National Acid Deposition Program
207 (NADP), the Global Precipitation Climatology Project (GPCP), the Parameter-elevation
208 Regressions on Independent Slopes Model (PRISM), and the Tropical Rainfall Measuring
209 Mission Multisatellite Precipitation Analysis (TMPA). The radiation and cloud data include
210 downward shortwave radiation at the ground surface (SWDOWN), net shortwave radiation at the
211 ground surface (GSW), downward longwave radiation at the ground surface (GLW), outgoing
212 longwave radiation at the top of the atmosphere (OLR), and shortwave and longwave cloud
213 forcing (SWCF and LWCF) from the Clouds and the Earth's Radiant Energy System (CERES);
214 aerosol optical depth (AOD), cloud fraction (CF), cloud water path (CWP), and cloud optical
215 thickness (COT) from the MODerate resolution Imaging Spectroradiometer (MODIS); and cloud
216 droplet number concentration (CDNC) derived based on MODIS data by Bennartz (2007). The
217 chemical data include surface O₃ from the Aerometric Information Retrieval System-Air Quality
218 Subsystem (AIRS-AQS) and the Clean Air Status and Trends Network (CASTNET); surface
219 particulate matter with 2.5 μm or less (PM_{2.5}) and its constituents including sulfate (SO₄²⁻),
220 nitrate (NO₃⁻), ammonium (NH₄⁺), elemental carbon (EC), organic carbon (OC), and total carbon
221 (TC = EC + OC) from the Interagency Monitoring of Protected Visual Environments
222 (IMPROVE) and the Chemical Speciation Network (CSN); surface particulate matter with
223 diameters of 10 μm or less (PM₁₀) from the AQS; and column abundance variables such as
224 column carbon monoxide (CO) from the Measurements of Pollution in the Troposphere

225 (MOPITT), tropospheric ozone residual (TOR) from the Ozone Monitoring Instrument (OMI),
226 and column nitrogen dioxide (NO₂) and formaldehyde (HCHO) from the Scanning Imaging
227 Absorption Spectrometer for Atmospheric Chartography (SCIAMACHY).

228 The satellite datasets used in this study are all level-3 gridded monthly-averaged data
229 with various resolutions (i.e., 0.25° for OMI and PRISM, 0.5° for SCIAMACHY, 1° for CERES,
230 GPCP, MODIS, and MOPITT). For the calculation of model performance statistics, the satellite
231 data with different resolutions are mapped to CMAQ's Lambert conformal conic projection
232 using bi-linear interpolation in the NCAR command language. CMAQ model outputs at
233 approximate time of the satellite overpass are paired with the satellite retrievals to facilitate a
234 consistent comparison. Note that only those grid points with valid satellite observations are
235 considered when paring model results with observations, and the averaging kernels are not
236 considered when analyzing the column CO and NO₂ results, which may introduce some
237 uncertainties (Wang et al., 2015b). Modeled CDNC is calculated as the average value of the
238 layer of low-level warm clouds between 950 and 850 hPa as suggested by Bennartz (2007).
239 Following the approach of Wielicki et al. (1996), the SWCF and LWCF are calculated as the
240 difference between the clear-sky and the all-sky reflected radiation at the top of atmosphere for
241 both simulations and observations.

242 The statistical performance evaluation follows a protocol similar to that of Zhang et al.
243 (2006, 2009a) and Yahya et al. (2016) and uses well-accepted statistical measures such as
244 correlation coefficient (R), mean bias (MB), root mean square error (RMSE), normalized mean
245 biases (NMB), and normalized mean error (NME) (S. Yu et al., 2006). Because of different
246 sampling protocols among monitoring networks, the evaluation is conducted separately for
247 individual networks for the same simulated variables/species.

248 3. Comprehensive model evaluation of two-way WRF-CMAQ

249 3.1 Meteorological evaluation

250 3.1.1 Surface meteorological variables

251 Figures 1 shows the spatial distribution of 5-year average MBs for T2, RH2, WS10, and
252 hourly precipitation from two-way WRF-CMAQ against the NCDC data in winter and summer,
253 2008-2012 and Tables 1 and 2 summarize the statistics for the same variables. Most variables
254 except for precipitation show overall moderate to good spatial performance with many sites
255 showing MBs within ± 1.0 °C for T2, ± 10 % for RH2, ± 1 m s⁻¹ for WS10, and ± 0.2 mm hr⁻¹ for
256 precipitation, respectively in both seasons. WRF-CMAQ tends to overpredict T2 (i.e., warm
257 bias) over widespread areas of domain especially along the Atlantic coast, the
258 eastern/southeastern U.S., the Central U.S., and Pacific coast in winter and underpredict T2 (i.e.,
259 cold bias) over the eastern U.S., the Central U.S., and mountainous U.S. in summer, which leads
260 to an overall small warm bias in the whole year (see Figure S1). Similar warm biases of T2 in
261 winter have been previously reported by Cohen et al. (2015) and are found to be associated with
262 the relatively deeper PBL depth using the non-local ACM2 PBL scheme. The relatively larger
263 warm/cold biases over coastal and mountainous areas are likely due to the coarse grid spacing of
264 36-km that cannot well resolve the complex topography (Yahya et al., 2016). Compared to many
265 previous WRF studies (Wang et al., 2012; Brunner et al., 2015; Yahya et al., 2016), which
266 typically show cold T2 biases, the overall small warm biases in this study can be attributed to the
267 soil moisture nudging technique used in the PX land surface scheme (Pleim and Gilliam, 2009).
268 The spatial patterns of MBs for RH2 show a general anti-correlation compared to T2 (i.e., RH2
269 is overpredicted where T2 is underpredicted and vice versa) due to the way how RH2 is

270 calculated based on T2. The spatial distribution of MBs for WS10 also shows dominant
271 overpredictions in both winter and summer especially along coastlines, indicating the prescribed
272 sea-surface temperature might not be sufficient to resolve the air-sea interactions. Systematic
273 overpredictions of hourly precipitation against NCDC data in both seasons are found to be
274 mainly caused by low non-convective precipitation events and can be attributed to the Morrison
275 microphysics scheme (Yahya et al., 2016).

276 The precipitation performance is further examined by comparing WRF-CMAQ with
277 TMPA and PRISM as shown in Figures 2. The spatial distribution of precipitation is well
278 simulated by WRF-CMAQ especially over the CONUS against observations by capturing the hot
279 spots along the Pacific Northwest coast in winter and some areas over the Central U.S. and FL in
280 summer. Moderate overpredictions of precipitation against TMPA over the Atlantic Ocean and
281 Gulf of Mexico in summer are also evident, possibly caused by overprediction of convective
282 precipitation by the Kain-Fritsch scheme (Hong et al., 2017) over ocean. As shown in Tables 1
283 and 2, the domain-average seasonal statistics demonstrate good performance for all variables
284 except for precipitation against NCDC in terms of MBs, NMBs, RMSE, and Rs. For example,
285 the MBs for T2, RH2, WS10, and precipitation are 1.1 °C, 2.2%, 0.57 m s⁻¹, and 0.05-0.23 mm
286 day⁻¹ (except for 0.71 mm day⁻¹ for NCDC) in winter and -1.1 °C, 3.7%, 0.38 m s⁻¹, and 0.13-
287 0.23 mm day⁻¹ (except for 0.75 mm day⁻¹ for NCDC) in summer, respectively, and Rs for those
288 variables are typically between 0.5-0.97, which are well within the performance benchmark
289 values recommended by Zhang et al. (2013) and Emery et al. (2017).

290 Figure 3 shows the bar charts of annual trends for T2, RH2, WS10, and precipitation in
291 2008-2012. Two-way WRF-CMAQ predicts the annual average T2 very well with MBs <
292 0.25 °C in all years. The simulation can also capture the increasing trend of T2 from 2008 to

293 2012 observed by NCDC. RH2 is consistently overpredicted by the two-way WRF-CMAQ in all
294 years despite relatively low biases (MBs < 3%). Both observations and simulations show the
295 lowest RH2 in 2012 and the highest in 2009. As also shown in Figure 1, the model tends to
296 systematically overpredict both WS10 and precipitation throughout all years as well. There are
297 no clear trends (i.e., increasing or decreasing) for WS10 and precipitation between 2008 to 2012
298 from either observations or simulations. However two-way WRF-CMAQ is able to capture both
299 the lowest wind speed and precipitation in 2012 and the highest wind speed in 2008 from
300 observations. In general, the model performs very well in reproducing the year-to-year variation
301 for the major meteorological variables between 2008 to 2012.

302 **3.1.2 Radiation and cloud variables**

303 Figures 4 and 5 compare the 5-year average spatial distribution of major radiation
304 variables (i.e., SWDOWN, GSW, GLW, OLR, and AOD) based on the satellite retrievals and
305 two-way WRF-CMAQ simulations in winter and summer, 2008-2012 and Tables 1 and 2
306 summarize the domain-average model performance statistics. WRF-CMAQ predicts the
307 longwave radiation variables GLW and OLR very well with domain-average of NMBs of -0.3%
308 and 1.8% in winter and -3.6% and 0.9% in summer, respectively, and Rs of 0.96 to 0.99 for both.
309 The shortwave radiation variables SWDOWN and GSW are slightly overpredicted on average
310 with NMBs of 11.3% and 7.5% in winter and 17.1% and 15.1% in summer, respectively, and Rs
311 ranging from 0.75 to 0.99 for both. The simulations also reliably reproduce the spatial
312 distribution of both longwave and shortwave radiation compared to observations in both seasons.
313 The relatively large overpredictions for shortwave radiation especially in summer are very likely
314 caused by the large underpredictions of aerosol direct radiative forcing reflected from the
315 underpredictions of AOD (Figure 5) as well as underprediction of indirect cloud radiative forcing

316 (see Figure 8). It has been reported that WRF v3.4 does not treat the subgrid cloud feedback to
317 radiation, which could also contribute to the overpredictions in shortwave radiation especially in
318 summer (Alapaty et al., 2012; Hong et al., 2017). The model largely underpredicts the magnitude
319 of AOD in both seasons (NMBs of -59.8% in winter and -67.8% in summer), while providing a
320 reasonable representation of the spatial distribution of AOD over the U.S., with generally higher
321 values over the Midwest in winter and over the eastern U.S. in summer. The model also
322 underpredicts the elevated AODs over oceans and the northern part of domain in both seasons.
323 Similar AOD underpredictions have been reported in previous studies over the U.S. using two-
324 way coupled WRF-CMAQ (Gan et al., 2015a; Hogrefe et al., 2015; Xing et al., 2015a). The
325 relatively large underpredictions of AOD may be caused by several factors. First,
326 underprediction of PM_{2.5} concentrations, particularly SO₄²⁻ in both seasons and OC in summer
327 (Tables 3 and 4), can contribute significantly to the underprediction of AOD, especially over the
328 eastern U.S. Second, the underestimation of dust emissions may contribute to missing hot spots
329 from the model over arid areas in CA and AZ (Zender et al., 2003) and underestimates of sea-salt
330 emissions may lead to missing elevated AODs over oceans (Gan et al., 2015b). Third, challenges
331 in adequately representing prescribed and wildfire emissions in the NEI (Kelly et al., 2019) may
332 cause many missing hot spots over large areas of the Pacific Northwest, CA, Canada, and the
333 eastern U.S. especially in summer. Fourth, uncertainties in BCONs of PM_{2.5} concentrations may
334 further contribute to underpredictions of AOD over oceans and the northern part of the domain.
335 For example, Kaufman et al. (2001) found that the background AOD could reach 0.1 over the
336 Pacific Northwest using Aerosol Robotic Network (AERONET) data. The AODs in the current
337 simulation seem to be biased low (between 0.02-0.06 in both seasons over the Pacific Ocean)
338 and indicate potential underpredictions of PM_{2.5} BCONs, especially in the free troposphere.

339 Finally, there are uncertainties associated with MODIS retrievals. Remer et al. (2005) found that
340 the uncertainty of level 3 MODIS monthly AODs can be up to $\pm 0.05 \pm 0.15$ AOD over the land
341 due to clouds and surface reflectance. More AOD data from other satellites or AERONET might
342 be considered in the future work to provide more robust ensemble type of evaluation for AOD.

343 Figures 6-8 compare the 5-year average spatial distribution of major cloud and cloud
344 radiative variables for the satellite retrievals and two-way WRF-CMAQ simulations in winter
345 and summer, 2008-2012 and Tables 1 and 2 summarize the corresponding statistics. As shown in
346 Figures 6 and 7, WRF-CMAQ tends to largely underpredict CDNC, COT, and CWP in both
347 seasons over most of the domain with the domain-average NMBs of -82.4%, -80.8%, and -45.3%
348 in winter and -79.2%, -83.6%, and -66.3% in summer, respectively. Despite the large
349 underprediction of those cloud variables, the spatial correlations are generally predicted well,
350 especially for COT and CWP with Rs ranging from 0.63 to 0.74. Compared to the other cloud
351 variables, CF is much better predicted with an NMB of -10.4% and an R of 0.87 in winter and an
352 NMB of -23.0% and an R of 0.81 in summer, respectively, which is consistent with the
353 performance reported in Yu et al. (2014). The model can reproduce the high CFs over northern
354 and northeastern part of domain as well as over oceans while capturing the low CFs over the
355 mountainous and plateau regions in the U.S. and Mexico especially in winter. In addition to the
356 underprediction of $PM_{2.5}$ (thus underestimating CCN), the large underpredictions of cloud
357 variables (especially CDNC and COT) can be attributed to uncertainties in aerosol microphysics
358 schemes (Yahya et al., 2016) as well as missing aerosol indirect effects on subgrid convective
359 clouds (Yu et al., 2014). Gantt et al. (2014) and Zhang et al. (2015b) also showed the aerosol
360 activation scheme (i.e., Abdul-Razzak and Ghan, 2000) used in the current version of WRF-
361 CMAQ may have underestimated CDNC and thus CWP and COT due to some missing processes

362 such as insoluble aerosol adsorption and giant cloud condensation nuclei. Overall, the relatively
363 poor model performance for cloud variables reflects current limitations in representing aerosol
364 indirect effects and aerosol-cloud interactions in state-of-science online coupled models. Further
365 model improvements that incorporate new knowledge from emerging studies should be
366 conducted in the future.

367 As shown in Figure 8, WRF-CMAQ predictions of SWCF and LWCF generally agree
368 well with the satellite observations in both seasons. The model can capture the elevated SWCF
369 and LWCF over the Atlantic Ocean and widespread areas over the eastern U.S. in winter and
370 those over the Pacific Northwest, northern part of the domain, and Atlantic Ocean in summer.
371 The domain-average NMBs are -11.1% for SWCF and -15.1% for LWCF in winter and -41.3%
372 for SWCF and -33.3% for LWCF in summer, respectively. The relatively larger biases in
373 summer compared to winter are correlated with larger biases associated with radiation and cloud
374 predictions potentially caused by larger underpredictions of aerosol predictions. As discussed
375 earlier, the underpredictions of SWCF may partially contribute the overprediction of SWDOWN
376 (more shortwave radiation reaching the ground) and those of LWCF may further lead to the
377 overpredictions in OLR (more longwave radiation emitted into the space). The performance of
378 SWCF and LWCF is consistent with the 12-km simulation reported in Yu et al. (2014) and even
379 slightly better in terms of NMBs, which might be associated with the long-term vs. short-term
380 simulations. It is also worth noting that SWCF (LWCF) is calculated as the difference between
381 the clear-sky and all-sky shortwave (longwave) radiation at the top of atmosphere, and so
382 performance for SWCF and LWCF depends on performance for both radiation and cloud
383 properties. The generally better performance in terms of model bias for SWCF and LWCF

384 compared to the cloud variables seems to be driven by the relatively good performance of
385 shortwave/longwave radiation in the model.

386 **3.2 Chemical evaluation**

387 **3.2.1 O₃**

388 Figure 9a shows the spatial distribution of simulated average daily maximum 8-h O₃ in
389 summer, 2008-2012 from two-way WRF-CMAQ overlaid with observations from both the
390 AIRS-AQS and CASTNET networks. WRF-CMAQ shows good performance by capturing the
391 spatial distribution of max 8-h O₃ over widespread areas of the domain. The model tends to
392 overpredict O₃ along coastlines in the southeastern U.S., Gulf of Mexico, and Pacific coast,
393 which can be attributed to a poor representation of coastal boundary layers (Yu et al., 2007) and
394 lack of O₃ sink via halogen chemistry (Sarwar et al., 2015) and deposition to water (Gantt et al.,
395 2017). The simulation also underpredicts O₃ in widespread areas in the Midwest, Central, and
396 mountainous regions of the U.S., which is consistent with the results of 36-km simulations from
397 Wang and Zhang (2012) that used an earlier version of CMAQ v4.6 with the same CB05 gas-
398 phase mechanism. In addition to cold T2 biases over those areas (Figure 1), the underpredictions
399 are also believed to be associated with inaccurate representations of precursor emissions and
400 elevated/complex terrain due to the coarse grid spacing of 36-km over those regions. Wang and
401 Zhang (2012) found that their 12-km simulation showed improved performance over similar
402 regions especially in summer.

403 Figure 9c shows the monthly variation of domain-average 5-year average O₃ mixing
404 ratios between observations from AIRS-AQS and simulations from two-way WRF-CMAQ, and
405 Figure 9d shows the diurnal variation of domain-average 5-year average hourly O₃ mixing ratios

406 between observations from CASTNET and simulations from two-way WRF-CMAQ for winter
407 and summer. As shown in Figure 9c, the O₃ mixing ratios are overpredicted throughout the year,
408 which is consistent with overprediction of T2 (figure not shown). The largest overprediction
409 occurs in the relatively cold months such as September to December. It is interesting that the
410 observations show the largest monthly O₃ mixing ratios in spring and early summer while the
411 simulation shows the peak during the summer. The difference in timing of peak O₃ between
412 observations and simulations during the year might be associated with uncertainties in the
413 BCONs of O₃ that reflect impacts of the long-range transport and associated stratosphere-
414 troposphere exchange of O₃. As shown in Figure 9d, WRF-CMAQ tends to overpredict O₃
415 during most hours (i.e., 2:00-18:00) in summer and throughout the whole day in winter partially
416 due to the overprediction of T2, especially in winter (Figure 1). The diurnal pattern of O₃ is
417 captured much better during summer with much less prediction bias, especially during the
418 nighttime, indicating that the model does a better job in predicting the evolution of nocturnal
419 boundary layer and atmospheric chemistry in the warm season than the cold season. The overall
420 overpredictions in this work are also consistent with previous studies (Eder and Yu, 2006; Appel
421 et al., 2007; Wang et al., 2012), although our results show much better nighttime performance
422 owing to the application of the ACM2 scheme that treats both local and non-local closure (Pleim,
423 2007). As also shown in Table 4, the domain-average NMBs and NMEs for max 8-h O₃ in
424 summer are 10.6% and 13.2% against AIRS-AQS and -3.0% and 11.5% against CASTNET,
425 respectively. The statistics are also consistent with previous studies using the CMAQ model
426 (Zhang et al., 2009a; Appel et al., 2013, 2017; Penrod et al., 2014) and can be considered as
427 good performance according to the criteria suggested by Zhang et al. (2013) and Emery et al.
428 (2017).

429 Figure 3 also shows the bar charts of annual trends for max 8-h O₃ from two-way WRF-
430 CMAQ against AQS and CASTNET observations in 2008-2012. Two-way WRF-CMAQ
431 systematically overpredicts O₃ especially against AQS data with MBs typically > 4.0 ppb. The
432 potential reasons for model biases have been discussed earlier in this section. There are no
433 obvious decreasing or increasing trends for max 8-h O₃ from AQS or CASTNET observations.
434 However, the model can generally capture the high O₃ mixing ratios in 2008 and 2010 and the
435 low O₃ mixing ratios in 2009 from both AQS and CASTNET. The similar down and up trends
436 between 2008 to 2010 for O₃ (i.e., decreasing from 2008 to 2009 and increasing from 2009 to
437 2010) from AQS observations were also found by Yahya et al. (2016), but not captured by their
438 simulations. Zhang and Wang (2016) was able to reproduce the similar trend over the
439 southeastern U.S. between 2008 to 2010 using their models and attributed the abnormal high
440 2010 O₃ mixing ratios to the extreme dry and warm weather conditions during fall 2010.

441 3.2.2 Aerosols

442 Figures 10a and 10c shows the spatial distribution of simulated 5-year average PM_{2.5}
443 from two-way WRF-CMAQ overlaid with observations from both the CSN and IMPROVE
444 networks in winter and summer, 2008-2012. As shown, WRF-CMAQ performs well for PM_{2.5}
445 over widespread areas of the Midwest and northeastern U.S. in both seasons, while PM_{2.5} is
446 underpredicted over the southeastern and western U.S. especially in winter. The model also
447 misses some hot spots of observed concentrations in the western U.S., which are mainly caused
448 by TC underpredictions (Figure S6) that are likely linked to poorly allocated and underestimated
449 wildfire emissions in the NEI (Wiedinmyer et al., 2006; Roy et al., 2007; Kelly et al., 2019). The
450 relatively large underpredictions over the eastern U.S. are mainly caused by the combined effects
451 from SO₄²⁻, NH₄⁺, and TC. As shown in Figure S6, WRF-CMAQ largely underpredicts SO₄²⁻ in

452 the Midwest and southeastern U.S. mainly due to the underprediction of oxidants such as O_3 (see
453 Figure 9a) (which leads to less production from the gaseous oxidation), overprediction of
454 precipitation (see Figure 2) (which leads to more wet deposition and removal), and large
455 underprediction of cloud fields (see Figures 6-7) (which leads to less aqueous phase formation),
456 over the same area. On the other hand, NH_4^+ and NO_3^- are either underpredicted or
457 overpredicted, respectively, over the similar areas mainly due to underprediction of SO_4^{2-} .
458 According to the aerosol thermodynamics, when SO_4^{2-} is underpredicted, NH_4^+ tends to be
459 underpredicted due to its major role as cation. More gaseous NH_3 will be available to neutralize
460 NO_3^- , thus leading to overprediction of NO_3^- especially over the sulfate poor regions (West et al.,
461 1999). Other potential reasons include the inaccurate assumptions in the thermodynamic module
462 (for example, the internally mixed aerosol state and equilibrium assumption may not be
463 representative over some regions and different time periods, S. Yu et al., 2006), uncertainties in
464 emissions of key species such as NH_3 and non-volatile cations that affect particle acidity (Mebust
465 et al., 2003; Wang and Zhang, 2014; Vasilakos et al., 2018; Pye et al., 2020), and measurement
466 errors especially for NO_3^- and NH_4^+ (X.-Y. Yu et al., 2006; Karydis et al., 2007; Wang and
467 Zhang, 2012). TC underpredictions over most sites of the domain can be attributed to the
468 underprediction of emissions (e.g., wildfire and primary OC) and underestimation of secondary
469 organic aerosol (SOA) formation (Appel et al., 2017; Pye et al., 2017) since EC (a chemically
470 inert species) is overpredicted, which suggest that atmospheric mixing did not drive the TC
471 underpredictions.

472 Figures 10e and 10f show the monthly variation of 5-year average $PM_{2.5}$ between
473 observations from CSN and IMPROVE, respectively, and simulations from two-way WRF-
474 CMAQ. Both observations and WRF-CMAQ show higher $PM_{2.5}$ concentrations at CSN than

475 IMPROVE for the whole year because most of CSN sites are in more polluted urban areas while
476 majority of IMPROVE sites are in rural areas and national parks. The model tends to
477 underpredict $PM_{2.5}$ over both CSN and IMPROVE sites in the warm months (i.e., April to
478 September) mainly due to the underpredictions of SO_4^{2-} and OC while it overpredicts $PM_{2.5}$ in
479 cold months mainly due to NO_3^- . The model also captures the seasonality of $PM_{2.5}$ better over
480 CSN sites than IMPROVE sites, especially in the summer months. The large underpredictions
481 over IMPROVE sites during summer months are likely due to the underestimation of precursor
482 emissions (such as wildfire emissions).

483 Figure 11 shows the scatter plots of major $PM_{2.5}$ components such as SO_4^{2-} , NH_4^+ , and
484 NO_3^- , and TC in winter and summer, 2008-2012. The WRF-CMAQ predicts $PM_{2.5}$ constituents
485 well with majority of data within the 1:2 ratio lines in both seasons. Systematic underpredictions
486 of SO_4^{2-} and NH_4^+ in winter and overpredictions of NO_3^- in summer are shown, which are
487 consistent with their spatial distributions. Relatively large under- and overpredictions of TC
488 especially in winter compensate each other and lead to relatively low overall model biases. As
489 also shown in Figure S6, the model fails to reproduce high concentrations of PM_{10} (those > 20
490 $\mu g m^{-3}$) over widespread areas of the domain, especially over dust source areas in CA, AZ, and
491 NM. Hong et al. (2017) found the similar large underprediction of dust using CMAQ v5.0.2 over
492 China and attributed it to a too-high threshold for friction velocity in the current dust module
493 (Dong et al., 2016). Sea-salt also seems to be underpredicted by WRF-CMAQ, although sea-salt
494 predictions are better than dust as shown along the coastlines.

495 Figure 3 shows the bar charts of annual averaged observations and simulations for $PM_{2.5}$
496 over the CSN and IMPROVE sites. Overall, the model performs well for $PM_{2.5}$ for most of years
497 and better over CSN than IMPROVE sites with general underpredictions in most years. The

498 observations for both CSN and IMPROVE show a general decreasing trend, ~~(except for 2010~~
499 ~~over CSN with a strong drop of PM_{2.5} concentrations.) especially over IMPROVE sites.~~
500 According to EPA (2012), the strong drop of PM_{2.5} in 2009 is due to a few reasons including
501 many national and local regulations that are imposed, the contribution of economic slowdown to
502 cleaner air conditions and also favorable meteorological conditions to lower air pollution levels
503 in 2009. The impacts are more apparent over CSN sites mainly composed of urban/suburban
504 areas than IMPROVE sites mainly composed of remote areas and national parks. Two-way
505 WRF-CMAQ is able to reproduce the declining trend well particularly over IMPROVE sites and
506 again demonstrate its capability in accurately simulating the year-to-year variations of not only
507 meteorology but air quality.

Formatted: Subscript

Formatted: Font: Not Bold

508 As recommended by some previous studies (Zhang et al., 2006; Wang and Zhang, 2012;
509 Emery et al., 2017), generally $\pm 15\%$ and $\pm 30\%$ for model biases and 30% and 50% for model
510 errors can be considered as good and acceptable performance. As shown in Tables 3 and 4,
511 WRF-CMAQ in this work demonstrates an overall good or acceptable performance in predicting
512 aerosols in terms of statistics especially for PM_{2.5} in both seasons, NO₃⁻ OC, and TC in winter,
513 and SO₄²⁻ and NH₄⁺ in summer. It shows the domain-average NMBs of -7.2% and 8.6% in winter
514 and -13.2% and -26.9% in summer for PM_{2.5} against CSN and IMPROVE, respectively; NMBs
515 of -10.2% and -20.9% in summer for SO₄²⁻ against CSN and IMPROVE, respectively; NMBs of
516 -0.3% and 13.3% in winter for NO₃⁻ against CSN and IMPROVE, respectively; an NMB of 3.3%
517 for NH₄⁺ in summer against CSN; an NMB of 13.0% in winter for OC against IMPROVE; and
518 NMBs of 7.2% and 17.5% in winter for TC against CSN and IMPROVE, respectively. The
519 relatively large underpredictions of PM₁₀ in both seasons, i.e., NMBs of -36.3% in winter and -
520 45.8% in summer against AQS, indicate further improvements of dust emissions are warranted.

521 Overall, the aerosol performance is also comparable or better than previous CMAQ or WRF-
522 CMAQ applications (Wang and Zhang, 2012; Penrod et al., 2014; Yu et al., 2014). For example,
523 Penrod et al. (2014) showed 5-year (2001-2005) average NMBs of -23.3% and 4.0% in winter
524 and -19.1% to -17.6% in summer for PM_{2.5} against CSN and IMPROVE data over the CONUS
525 using the CMAQ v5.0 and Yu et al. (2014) reported the monthly mean NMBs of -6.2% and -
526 16.8% for PM_{2.5} against CSN and IMPROVE over the eastern U.S. using the same version of
527 WRF-CMAQ as that used in this study.

528 3.2.3 Column abundance

529 Figures 12 and 13 show the spatial distribution of 5-year average column abundances
530 between various satellite products and two-way WRF-CMAQ for column CO, TOR, column
531 NO₂, and column HCHO in winter and summer, 2012 and Tables 3 and 4 summarize the
532 statistics. As shown, WRF-CMAQ can reproduce the spatial distribution of the column
533 abundances of gases quite well in both seasons except for column HCHO in winter with Rs
534 ranging from 0.70 to 0.87. TOR in both seasons, column NO₂ in winter and column HCHO in
535 summer are also generally well predicted in terms of magnitudes with NMBs of 4.7% for TOR
536 and 0.3 for NO₂, respectively, in winter and -8.0% for TOR and 15.0% for HCHO,
537 respectively, in summer. Systematic underpredictions for column CO occur in both seasons over
538 the whole domain with NMBs of -20.5% in winter and -27.8% in summer for a few reasons.
539 First, the BCONs of CO may be significantly underestimated from the CESM model. Using
540 WRF/Chem or its variant, Zhang et al. (2016b, 2019) found that the column CO performance
541 could be greatly improved by adjusting the BCON using the satellite observation. A similar
542 approach could be applied in future WRF-CMAQ simulations as well. Second, as pointed by
543 Heald et al. (2003), the regional emissions, especially biomass burning, could be a significant

544 source for elevated CO concentrations and thus underestimation of these emissions could
545 contribute to the CO underprediction. A more robust set of fire emissions from FINN generated
546 by NCAR based on satellite retrievals has been applied to the similar time period recently but
547 using the WRF-Chem model (Zhang and Wang, 2019) and were found to improve the column
548 CO performance. Last, Emmons et al. (2009) showed positive biases (i.e., 19%) of MOPITT
549 retrievals over the land when compared to in-situ measurements and the biases may have been
550 increasing over time due to the MOPITT bias drift (e.g., 0.5% yr⁻¹ for version 7 retrieval). The
551 predicted TOR can capture the observed high values over the eastern U.S. and oceans and the
552 low values in elevated terrain especially in summer and it shows the best performance among all
553 gas species. Both satellite observations and simulations can capture the elevated column NO₂
554 over the industrial and metropolitan areas in the domain where large nitrogen oxide (NO_x)
555 emission sources are located especially in winter. The model shows moderate underprediction
556 with an NMB of -27.8% in summer which can be attributed to both uncertainties in the emissions
557 and satellite retrievals. For example, the lightning emissions of NO_x are missing from this study,
558 which have been found by previous studies (Allen et al., 2012) to contribute up to 2.0×10^{15}
559 molecules cm⁻² over the southern U.S., the Gulf of Mexico, and northern Atlantic Ocean during
560 the summer. Boersma et al. (2004) also found that different column NO₂ retrieval approaches
561 may lead to large errors (> 25%) over polluted areas. Column HCHO over the CONUS
562 especially the southeastern U.S. is well predicted in summer in terms of both magnitude and
563 spatial distribution and correlates well with the biogenic emission source regions. The
564 underprediction of column HCHO in winter may indicate potential underestimation of
565 anthropogenic emissions. Other reasons including potential low yield of HCHO from isoprene
566 and terpene in the CB05 mechanism and uncertainties in satellite retrievals (Stavrakou et al.,

567 2009; Lorente et al., 2017). For example, According to Stavrakou et al. (2009), the air mass
568 factors used for HCHO column calculation may bear ~18% error under clear sky conditions to
569 ~50% error for very cloudy conditions. The winter typically has higher cloud cover than summer
570 (See Figs. 6 and 7) and thus higher uncertainties for HCHO column.

Formatted: Font: Not Bold

571 3.2.4 Simulated O₃ and PM_{2.5} exceedances of NAAQS levels

572 National Ambient Air Quality Standards (NAAQS) are set for criteria pollutants,
573 including O₃ and PM_{2.5}, to provide protection against adverse health and welfare effects
574 (www.epa.gov/criteria-air-pollutants/naaqs-table). In this section, the average number of days
575 per year where the 24-hr PM_{2.5} NAAQS level (35 µg m⁻³) and the max 8-h O₃ NAAQS level (70
576 ppb) are exceeded from the WRF-CMAQ predictions is compared with the number of
577 exceedances in the monitoring data (i.e., O₃ from AQS and CASTNET and PM_{2.5} from
578 IMPROVE and CSN). This comparison is intended to better characterize the ability of the model
579 to simulate the high-concentration days that could be especially relevant in regulatory
580 assessments. In Figure 14, the five-year average of the annual number of exceedance days is
581 shown for WRF-CMAQ and the monitoring data at monitor locations. As shown, the
582 observations indicate a large number of annual exceedance days for max 8-h O₃ over major
583 cities, especially in CA, TX, the Midwest, and northeastern U.S. The spatial distribution of the
584 observed number of exceedance days from the AQS and CASTNET networks aligns well with
585 the nonattainment map reported by the Green Book of U.S. EPA ([https://www.epa.gov/green-](https://www.epa.gov/green-book)
586 [book](https://www.epa.gov/green-book)). The WRF-CMAQ model also captures the distribution of the number of exceedance days
587 very well, especially in CA and northeastern U.S. The domain-average values of NMB, NME,
588 and R are -3.4%, 14.0%, and 0.98, respectively, also indicating a good performance. For PM_{2.5},
589 the largest number of exceedance days based on the IMPROVE and CSN observations mainly

590 occurs in the northwestern U.S., Midwest, and major cities in the northeastern U.S. The number
591 of exceedance days is generally much lower for PM_{2.5} than O₃. The spatial distribution of the
592 number of exceedance days for observed PM_{2.5} aligns well with nonattainment areas reported by
593 the Green Book from U.S. EPA in CA. However, the number of simulated PM_{2.5} exceedance
594 days underpredicts the observation-based values in the western U.S. mainly due to large
595 underpredictions of PM_{2.5} concentrations in the same areas as shown in Figure 10. The
596 simulation better predicts the distribution of the number of exceedance days in the eastern U.S.
597 where terrain is relatively flat and wildfire less prevalent. The domain-average values of NMB,
598 NME, and R are -29.0%, 80.8%, and 0.21, respectively.

599 **4. Impacts of chemistry-meteorology feedbacks**

600 In this section, the impacts of chemistry-meteorology feedbacks including aerosol direct
601 and indirect effects on regional meteorology and air quality over the U.S. are further examined
602 by comparing results from two-way WRF-CMAQ and offline coupled WRF and CMAQ. Model
603 performance from the two sets of simulations is first compared to demonstrate the potential
604 performance improvements of the two-way model, and the impacts on regional meteorology and
605 air quality are further investigated via the spatial difference plots for selected variables and
606 species.

607 **4.1 Meteorology**

608 Figures 2 and 8 compare observations and simulations from the two-way WRF-CMAQ
609 and WRF-only models for precipitation and SWCF/LWCF, respectively. Tables 1 and 2 also
610 summarize the model performance statistics for all major meteorological variables for the two
611 simulations. The statistics of some cloud variables from the WRF-only simulation are not

612 available due to missing model outputs. Overall, good performance is evident for both
613 simulations for surface meteorological variables with slightly better performance for most of
614 variables (except for RH2 in both seasons and T2 in summer) for the two-way WRF-CMAQ
615 simulation than the WRF-only simulation. The MBs for the two-way WRF-CMAQ vs. WRF-
616 only simulation are 1.1 °C vs 1.2 °C for T2, 2.2% vs 2.1% for RH2, 0.57 m s⁻¹ vs 0.58 m s⁻¹ for
617 WS10, 16.7 degree vs 16.9 degree for WD10, and 0.05-0.71 mm day⁻¹ vs 0.04-0.72 mm day⁻¹ for
618 precipitation in winter and -1.1 °C vs -0.9 °C for T2, 3.7% vs 3.2% for RH2, 0.38 m s⁻¹ vs 0.42
619 m s⁻¹ for WS10, 49.1 degree vs 49.8 degree for WD10, and 0.13-0.75 mm day⁻¹ vs 0.19-0.9 mm
620 day⁻¹ for precipitation in summer. The spatial distributions for SWCF and LWCF are better
621 captured in both seasons especially over the eastern U.S., Atlantic Ocean, and Gulf of Mexico in
622 winter and over the Midwest and Pacific Northwest in summer. Compared to WRF-only, two-
623 way WRF-CMAQ shows noticeably better performance in terms of both MB and RMSE for
624 radiation and cloud forcing, with MBs of 11.3 vs. 19.5 W m⁻² for SWDOWN, 7.5 vs 14.1 W m⁻²
625 for GSW, -0.9 vs. -6.3 W m⁻² for GLW, 4.0 vs. 4.7 W m⁻² for OLR, -3.0 vs. -7.4 W m⁻² for
626 SWCF, and -3.3 vs. -4.1 W m⁻² for LWCF in winter and with MBs of 43.6 vs. 59.4 W m⁻² for
627 SWDOWN, 33.6 vs 47.2 W m⁻² for GSW, -13.4 vs. -16.8 W m⁻² for GLW, 2.3 vs. 3.0 W m⁻² for
628 OLR, -22.8 vs. -31.1 W m⁻² for SWCF, and -8.6 vs. -9.0 W m⁻² for LWCF in summer. These
629 results are consistent with those reported by Yahya et al. (2015a,b) that showed similar
630 improvements in meteorological and radiative variables when comparing predictions from WRF-
631 Chem with those from WRF only. Since identical inputs and physics options are used in both
632 simulations, the differences in performance for meteorological variables is due to the
633 consideration of feedback processes among chemistry, aerosol, cloud, and radiation in the two-
634 way coupled WRF-CMAQ simulation.

635 Figure 15 shows the 5-year average difference plots of selected major meteorological
636 variables including SWDOWN, T2, RH2, WS10, PBL height, and precipitation between two-
637 way WRF-CMAQ and WRF-only in 2008-2012. As shown, the incoming shortwave radiation is
638 reduced by up to 24.8 W m^{-2} (13.6%) with a domain-average of 13.0 W m^{-2} (6%) due to the
639 combined aerosol direct and indirect radiative effects over the domain. The reduction is
640 predominant over the eastern U.S. where both aerosol loading and cloud cover are high and over
641 the oceans where cloud cover is high. The magnitude of shortwave radiation reduction in this
642 work is consistent with other studies. For example, Wang et al. (2015a) found that the combined
643 aerosol direct and indirect effects using the WRF/Chem model, which includes the sub-scale
644 cloud forcing not treated in the current WRF-CMAQ model, may decrease the incoming
645 shortwave radiation by 16.0 W m^{-2} in the summer over the U.S. Hogrefe et al. (2015) reported
646 the reduction of shortwave radiation may reach up to 20 W m^{-2} over the eastern U.S. by only
647 considering the aerosol direct effect using an older version of WRF-CMAQ v5.0.1. Xing et al.
648 (2015b) showed that the aerosol direct forcing may cause the surface shortwave radiation to
649 decrease by up to 10 W m^{-2} over the eastern U.S. over a decadal time period using WRF-CMAQ
650 v5.0. The reduction of shortwave radiation further reduces the surface temperature by up to
651 $0.25 \text{ }^{\circ}\text{C}$ over the eastern U.S., which is much larger than the reduction of $0.1 \text{ }^{\circ}\text{C}$ reported by
652 Hogrefe et al. (2015), mainly due to the inclusion of aerosol indirect effects. However there are
653 smaller reductions of T2 over the Pacific Ocean and even increases (by up to $0.1 \text{ }^{\circ}\text{C}$) over large
654 areas of Atlantic Ocean and Gulf of Mexico where much larger reductions of shortwave radiation
655 occur. As pointed by Wang et al. (2015a), due to the much larger heat capacity of ocean, the
656 response of sea surface temperature is less sensitive to the change of shortwave radiation for
657 ocean compared to the land. The large increase of incoming longwave radiation and latent heat

658 (figures not shown) caused by the aerosol indirect effects and other complex feedback processes
659 over the ocean compensates for the reduction of shortwave radiation, especially over the Atlantic
660 Ocean and Gulf of Mexico, and thus leads to less reduction or even increases of T2. RH2 is
661 found to mostly increase by 3.4% over the land caused by the decrease of temperature while
662 decrease by 2.6% over the ocean caused by either the increase of temperature or large decrease
663 of water vapor. Over the land, the decreases in shortwave radiation and temperature along with
664 the latent heat (figure not shown) lead to a more stable PBL and thus suppress the wind (by
665 reducing the wind speed as shown). Over the ocean, the changes lead to a more unstable PBL
666 and thus enhance the wind over the ocean. The wind speed and PBL height are reduced by up to
667 0.05 m s^{-1} and 25 m, respectively, over the U.S. The aerosol feedbacks on precipitation are also
668 mixed with relatively large decreases by up to 0.4 mm day^{-1} over the U.S. and increases by up to
669 0.4 mm day^{-1} over oceans. The suppression of precipitation over the land is mainly due to the
670 formation of more small sized CCNs caused by aerosol indirect effects and align well with areas
671 with high aerosol loadings while the enhancement of precipitation, especially along coastlines
672 and over oceans, might be associated with the larger CCN formation via more activated sea-salt
673 particles as indicated by Zhang et al. (2010) and Wang et al. (2015a).

674 **4.2 Air Quality**

675 Figures 9-11 compare observations and simulations from two-way WRF-CMAQ and
676 offline CMAQ for O_3 , $\text{PM}_{2.5}$, and $\text{PM}_{2.5}$ constituents. Tables 3 and 4 summarize the statistics for
677 all major chemical variables for the two simulations. As shown in Figure 9, two-way WRF-
678 CMAQ shows better performance for both the monthly variation of O_3 (throughout the whole
679 year) over AQS sites and the diurnal pattern of O_3 (especially during winter) over CASTNET
680 sites due to better performance of T2 and radiation compared to offline WRF and CMAQ. As

681 shown in Figure 10, two-way WRF-CMAQ shows better spatial distribution of PM_{2.5} in winter
682 and similar one in summer and better performance for PM_{2.5} for most of months over CSN sites
683 and for cold seasons across IMPROVE sites compared to offline CMAQ. Figure 11 shows
684 systematically better performance for SO₄²⁻, NO₃⁻, NH₄⁺, and TC with more data within 1:2 or
685 closer to 1:1 ratio lines of scatter plots in both seasons. Overall, as shown in Tables 3 and 4, both
686 simulations show generally good performance for all major chemical species except for PM₁₀.
687 For example., the domain-average NMBs are 10.6% (AQS) and -3.0% (CASTNET) vs. 14.2%
688 (AQS) and 0.2% (CASTNET) for O₃ in summer, -7.2% (CSN) and 8.6% (IMPROVE) vs. 1.8%
689 (CSN) and 23.7% (IMPROVE) for PM_{2.5} in winter and -13.2% (CSN) and -26.9% (IMPROVE)
690 vs. -14.0% (CSN) and -22.8% (IMPROVE) for PM_{2.5} in summer for two-way WRF-CMAQ and
691 offline-coupled CMAQ, respectively. The two-way WRF-CMAQ shows better domain-wide
692 statistics in terms of both correlation and biases for many variables including O₃, SO₄²⁻, NO₃⁻,
693 and EC as well as TOR and column NO₂ in both seasons, apparently due to the treatment of
694 chemistry-meteorology feedbacks. Offline CMAQ performs better for total PM_{2.5} especially in
695 the western U.S. due to higher dust emissions from higher wind speed and higher SOA due to
696 stronger radiation and higher temperature. However more robust comparisons are needed in the
697 future with improved dust emissions and the use of FINN wildfire emissions.

698 Figure 16 shows the 5-year average difference plots of selected chemical variables
699 including CO, O₃, NO_x, volatile organic compounds (VOCs), SO₄²⁻, SOA, PM_{2.5}, and PM₁₀
700 between two-way WRF-CMAQ and offline-coupled CMAQ. As shown, the CO mixing ratios
701 decrease by up to 79.2 ppb (27.8%) especially over the western U.S. with a domain-average
702 reduction of 3.0 ppb (3.1%) due to reduced formation of CO from the oxidation of VOCs caused
703 by reduced solar radiation as indicated by Zhang et al. (2017). Such reductions seem to dominate

704 over the increases caused by reduced PBL height, especially in the western U.S. where PBL
705 height reductions are minimum. The O₃ mixing ratios decrease by up to 5.2 ppb (16.2%) with
706 domain-average of 1.7 ppb (4.2%) mainly due to the reduced solar radiation and T2. The change
707 of O₃ is consistent with other studies such as Makar et al. (2015) and Wang et al. (2015a) that
708 also reported lower O₃ mixing ratios caused by aerosol direct and indirect effects. On the other
709 hand, both NO_x and VOC mixing ratios increase over the eastern U.S. while they decrease over
710 the western U.S. The increase should be caused by the combination of the large reduction of PBL
711 mixing and reduced solar radiation which reduces NO₂ photolysis and VOC oxidation to SOA.
712 For aerosol species, SO₄²⁻ concentrations increase by up to 0.38 μg m⁻³ (26.6%) especially over
713 the eastern U.S. In fact, the decrease of O₃ mixing ratios caused by feedbacks is expecting to
714 reduce SO₄²⁻ production via the gas-phase oxidation pathway due to the influence of O₃ on OH,
715 but increase SO₄²⁻ production via the aqueous-phase chemistry pathway due to more clouds in
716 the two-way WRF-CMAQ simulation. Thus, the net increase of SO₄²⁻ is more dominate by the
717 aqueous-phase chemistry instead of the gas-phase oxidation. This net increase of SO₄²⁻, in turn,
718 leads to an increase of NH₄⁺ and decrease of NO₃⁻ (figures not shown) through aerosol
719 thermodynamic equilibrium. SOA concentrations decrease by up to 0.34 μg m⁻³ (41.6%)
720 especially over the eastern U.S. due to the large reduction of oxidants. PM_{2.5} concentrations also
721 decrease by up to 5.2 μg m⁻³ (49.1%) with a domain-average of 0.34 μg m⁻³ (8.6%), and PM₁₀
722 concentrations decrease by up to 19.3 μg m⁻³ (64.8%) with a domain-average of 1.1 μg m⁻³
723 (11.1%). The reductions are more apparent over the western U.S. than the eastern U.S. partially
724 due to the compensation of the increase of SO₄²⁻ and NH₄⁺ and decrease of other secondary
725 aerosols over the eastern U.S., as well as the relatively large reduction of dust concentrations
726 over the western U.S. caused by reduced wind speed.

727 **5. Summary and conclusion**

728 In this study, two sets of long-term simulations for 2008-2012 using the two-way coupled
729 WRF-CMAQ and offline coupled WRF and CMAQ, respectively, are conducted, evaluated, and
730 compared to investigate the performance improvements due to chemistry-meteorology feedbacks
731 and impacts of those feedbacks on the regional air quality in the U.S. First, the two-way coupled
732 WRF-CMAQ simulation with both aerosol direct and indirect radiative forcing is
733 comprehensively evaluated in both winter and summer seasons and the annual trend is examined
734 between observations and simulations for selected major variables. The results show that WRF-
735 CMAQ performs well for major surface meteorological variables such as temperature at 2 m,
736 relative humidity at 2 m, wind speed at 10 m, and precipitation with domain-average MBs of -
737 1.1-1.1 °C, 2.2-3.7%, 0.38-0.57 m s⁻¹, and 0.13-0.23 mm day⁻¹ (except for 0.71-0.75 mm day⁻¹
738 against NCDC), respectively, in winter and summer. The relatively large positive biases for
739 precipitation are found to be more apparent when observed precipitation is low (dominated more
740 by the non-convective precipitation) and are thus believed to be more associated with
741 uncertainties in the Morrison microphysics scheme. The long-term simulation also shows
742 generally good performance for major radiation and cloud radiative variables. Relatively large
743 model biases still exist for cloud variables such as CDNC, COT, and CWP, indicating that the
744 processes associated with aerosol indirect effects are still not well understood and an accurate
745 simulation of those effects is still challenging using state-of-the-science models. WRF-CMAQ
746 can also capture the observed year-to-year variations well for almost all the major meteorological
747 and chemical variables.

748 Two-way WRF-CMAQ also shows generally good or acceptable performance for max 8-
749 h O₃, PM_{2.5} and PM_{2.5} constituents, with NMBs generally within ±15% for O₃ and ±30% for

750 PM_{2.5} species. For example, the domain-average NMBs are 10.6 % and -3.0 % for max 8-h O₃
751 against AQS and CASTNET in summer and -13.2 to -7.2 % and -26.9 to 8.6 % for PM_{2.5} against
752 CSN and IMPROVE in both seasons. O₃ mixing ratios are overpredicted for most months,
753 especially in the winter, in part due to the larger overprediction of T2 during the cold season. The
754 overall model biases are small for PM_{2.5} due to the compensation of relatively large
755 underpredictions of SO₄²⁻ and OC, especially in the warm season, and overprediction of NO₃⁻ in
756 the cold season. In addition to biases inherited from the meteorology, the model performance for
757 chemistry also suffers from uncertainties associated with emissions, the use of a coarse spatial
758 resolution, and representation of aerosol formation pathways in the model. For example, the
759 relatively large biases for EC might be associated with poorly allocated anthropogenic/wildfire
760 emissions and those for OC might be due to underestimation of SOA formation in version 5.0.2
761 of CMAQ. WRF-CMAQ also predicts the column abundances of chemical species well and the
762 relatively large model biases for CO are found to be associated with an underestimation of
763 BCONs. The model better reproduces the observed number of exceedance days for O₃ than
764 PM_{2.5} mainly due to better performance for O₃ than PM_{2.5} concentrations.

765 The performance comparison between two-way WRF-CMAQ and WRF-only simulations
766 shows that two-way WRF-CMAQ model performs better for major surface meteorological,
767 radiation, and cloud radiative variables due to the consideration of chemistry-meteorology
768 feedbacks associated with aerosol direct and indirect forcing. The feedbacks are found to reduce
769 the 5-year average SWDOWN by up to 24.8 W m⁻², T2 by up to 0.25 °C, PBL height by up to 25
770 m, wind speed by up to 0.05 m s⁻¹, and precipitation by up to 0.4 mm day⁻¹ over the CONUS,
771 which in turn affect the air quality significantly. As a result of feedbacks, two-way WRF-CMAQ
772 outperforms offline CMAQ for O₃, SO₄²⁻, NO₃⁻, NH₄⁺, and EC as well as TOR and column NO₂

773 in terms of both spatiotemporal variations and domain-average statistics due to better
774 meteorology performance for variables such as T2, WS10, radiation, and precipitation. Despite
775 these improvements, the offline CMAQ performs better for total PM_{2.5} in terms of domain-
776 average statistics, which could be partially caused by the compensation of larger under- and
777 over-predictions of PM_{2.5} constituents. More robust comparison for PM_{2.5} should be performed
778 with improved dust and wildfire emissions in future work. Chemistry-meteorology feedbacks are
779 found to play important roles in affecting U.S. air quality by reducing domain-wide 5-year
780 average surface CO by 3.0 ppb (3.1%) and up to 79.2 ppb (27.8%), O₃ by 1.7 ppb (4.1%) and up
781 to 5.2 ppb (16.2%), PM_{2.5} by 0.34 μg m⁻³ (8.6%) and up to 5.2 μg m⁻³ (49.1%), and PM₁₀ by 1.1
782 μg m⁻³ (11.1%) and up to 19.3 μg m⁻³ (64.8%) mainly due to reduction of radiation, temperature,
783 and wind speed.

784 In summary, the two-way coupled WRF-CMAQ modeling in this study shows generally
785 satisfactory and consistent performance for the long-term prediction of regional meteorology and
786 air quality when compared to other studies in the literature. Possible causes for the
787 meteorological and chemical biases that were identified through this work can provide valuable
788 information for future model development to improve the two-way coupled WRF-CMAQ model
789 and those biases should also be considered when making future climate/air quality projections.
790 Non-negligible model improvements for many major meteorological and chemical variables
791 compared to the traditional application of offline coupled WRF and CMAQ suggest the
792 importance of chemistry-meteorology feedbacks, especially aerosol direct and indirect effects.
793 The feedbacks should be considered along with other factors in developing future model
794 applications to inform policy making.

795 **Code Availability**

796 The modeling system used in this study is based on the 2-way coupled WRF-CMAQ model
797 derived from WRF v3.4 and CMAQ v5.0.2. Relevant code for CMAQ v5.0.2, its coupling to
798 WRF and aerosol direct feedbacks are publicly available from: doi:10.5281/zenodo.1079898.
799 WRF v3.4 code can be downloaded from
800 http://www2.mmm.ucar.edu/wrf/users/download/get_source.html. The version of the coupled
801 WRF-CMAQ model with the additional indirect aerosol forcing approach of Yu et al. (2014) can
802 be downloaded from the following website: <https://person.zju.edu.cn/shaocaiyu#674502>.

803 **Author contribution**

804 YZ and MB defined the scope of the manuscript. YZ and KW designed all the simulations. SY
805 and DW developed the two-way coupled WRF-CMAQ code. KW conducted all the simulations
806 and performed the analyses. KW drafted the manuscript. YZ, SY, DW, JP, RM, JK, and MB
807 reviewed and edited the manuscript.

808 **Competing interests**

809 The authors declare that they have no conflict of interest.

810 **Acknowledgements**

811 This work was developed at North Carolina State University and Northeastern University under
812 Assistance Agreement No. RD835871 awarded by the U.S. Environmental Protection Agency to
813 Yale University. The views expressed in this manuscript are those of the authors alone and do
814 not necessarily reflect the views and policies of the U.S. Environmental Protection Agency. EPA
815 does not endorse any products or commercial services mentioned in this publication. High
816 performance computing was support from Yellowstone (ark:/85065/d7wd3xhc) provided by

817 NCAR's CISL, sponsored by the NSF and the Stampede XSEDE high-performance computing
818 support under the NSF ACI-1053575. The work of S. Yu is supported by the Department of
819 Science and Technology of China (No. 2016YFC0202702, 2018YFC0213506 and
820 2018YFC0213503), National Research Program for Key Issues in Air Pollution Control in China
821 (No. DQGG0107) and National Natural Science Foundation of China (No. 21577126 and
822 41561144004). The authors gratefully acknowledge the availability of CERES, GPCP, MODIS,
823 MOPITT, NCDC, OMI, PRISM, SCHIAMACHY, and TMPA data. The authors thank Dr. Ralf
824 Bennartz from Vanderbilt University for providing the CDNC data. The authors also would like
825 to thank Drs. Jerry Herwehe and Shannon Koplitz from the U.S. EPA for their constructive and
826 very helpful comments.

827 **References**

- 828 Abdul-Razzak, H. and Ghan, S. J.: A parameterization of aerosol activation 2. Multiple aerosol
829 types, *J. Geophys. Res.*, 105 (D3), 6837-6844, 2000.
- 830 Alapaty, K., Herwehe, J. A., Otte, T. L., Nolte, C. G., Bullock, O. R., Mallard, M. S., Kain, J. S.,
831 and Dudhia, J.: Introducing subgrid-scale cloud feedbacks to radiation for regional
832 meteorological and climate modeling, *Geophys. Res. Lett.*, 39, L24809,
833 <https://doi.org/10.1029/2012GL054031>, 2012.
- 834 Allen, D. J., Pickering, K. E., Pinder, R. W., Henderson, B. H., Appel, K. W., and Prados, A.:
835 Impact of lightning-NO on eastern United States photochemistry during the summer of 2006 as
836 determined using the CMAQ model, *Atmos. Chem. Phys.*, 12, 1737-
837 1758, <https://doi.org/10.5194/acp-12-1737-2012>, 2012.
- 838 Appel, K. W., Gilliland, A. B., Sarwar, G., and Gilliam, R. C.: Evaluation of the Community
839 Multiscale Air Quality (CMAQ) model version 4.5: Sensitivities impacting model performance:
840 Part I, Ozone, *Atmos. Environ.*, 41, 9603-9615, 2007.
- 841 Appel, K. W., Pouliot, G. A., Simon, H., Sarwar, G., Pye, H. O. T., Napelenok, S. L., Akhtar, F.,
842 and Roselle, S. J.: Evaluation of dust and trace metal estimates from the Community Multiscale
843 Air Quality (CMAQ) model version 5.0, *Geosci. Model Dev.*, 6, 883-899,
844 <https://doi.org/10.5194/gmd-6-883-2013>, 2013.
- 845 Appel, K. W., Napelenok, S. L., Foley, K. M., Pye, H. O. T., Hogrefe, C., Luecken, D. J., Bash,
846 J. O., Roselle, S. J., Pleim, J. E., Foroutan, H., Hutzell, W. T., Pouliot, G. A., Sarwar, G., Fahey,

847 K. M., Gantt, B., Gilliam, R. C., Heath, N. K., Kang, D., Mathur, R., Schwede, D. B., Spero, T.
848 L., Wong, D. C., and Young, J. O.: Description and evaluation of the Community Multiscale Air
849 Quality (CMAQ) modeling system version 5.1, *Geosci. Model Dev.*, 10, 1703–1732,
850 <https://doi.org/10.5194/gmd-10-1703-2017>, 2017.

851 Baklanov, A., Schlünzen, K. H., Suppan, P., Baldasano, J., Brunner, D., Aksoyoglu, S.,
852 Carmichael, G., Douros, J., Flemming, J., Forkel, R., Galmarini, S., Gauss, M., Grell, G., Hirtl,
853 M., Joffre, S., Jorba, O., Kaas, E., Kaasik, M., Kallos, G., Kong, X., Korsholm, U., Kurganski,
854 A., Kushta, J., Lohmann, U., Mahura, A., Manders-Groot, A., Maurizi, A., Moussiopoulos, N.,
855 Rao, S. T., Savage, N., Seigneur, C., Sokhi, R. S., Solazzo, E., Solomos, S., Sørensen, B.,
856 Tsegas, G., Vignati, E., Vogel, B., and Zhang, Y.: Online coupled regional meteorology-
857 chemistry models in Europe: Current status and prospects, *Atmos. Chem. Phys.*, 14, 317–398,
858 [doi:10.5194/acp-14-317-2014](https://doi.org/10.5194/acp-14-317-2014), 2014.

859 Bennartz, R.: Global assessment of marine boundary layer cloud droplet number concentration
860 from satellite, *J. Geophys. Res.*, 112, D02201, <http://dx.doi.org/10.1029/2006JD007547>, 2007.

861 Boersma, K. F., Eskes, H. J., and Brinkma, E. J.: Error analysis for tropospheric NO₂ retrieval
862 from space, *J. Geophys. Res.*, 109, D04311, [doi:10.1029/2003JD003962](https://doi.org/10.1029/2003JD003962), 2004.

863 Brunner, D., Savage, N., Jorba, O., Eder, B., Giordano, L., Badia, A., Balzarini, A., Baro, R.,
864 Bianconi, R., Chemel, C., Curci, G., Forkel, R., Jimenez-Guerrero, P., Hirtl, M., Hodzic, A.,
865 Hozak, L., Im, U., Knote, C., Makar, P., Manders-Groot, A., van Meijgaard, E., Neal, L., Perez,
866 J. L., Pirovano, G., San Jose, R., Schroder, W., Sokhi, R. S., Syrakov, D., Torian, A., Tuccella,
867 P., Werhahn, J., Wolke, R., Yahya, K., Zabkar, R., Zhang, Y., Hogrefe, C., and Galmarini, S.:
868 Comparative analysis of meteorological performance of coupled chemistry-meteorology models
869 in the context of AQMEII phase 2, *Atmos. Environ.*, 115, 470–498,
870 [doi:10.1016/j.atmosenv.2014.12.032](https://doi.org/10.1016/j.atmosenv.2014.12.032), 2015.

871 Byun, D. W. and Schere K. L.: Review equations, computational algorithms, and other
872 components of the Models-3 Community Multi-Scale Air Quality (CMAQ) modeling system,
873 *Applied Mechanics Reviews*, 59(2), 51–77, [doi:10.1115/1.2128636](https://doi.org/10.1115/1.2128636), 2006.

874 Choi, M.W., Lee, J. H., Woo, J. W., Kim, C. H., and Lee, S. H.: Comparison of PM_{2.5} chemical
875 components over East Asia simulated by the WRF-Chem and WRF/CMAQ models: On the
876 models' prediction inconsistency, *Atmosphere*, 10, 618, 2019.

877 Cohen, A. E., Cavallo, S. M., Coniglio, M. C., and Brooks, H. E.: A review of planetary
878 boundary layer parameterization schemes and their sensitivity in simulating southeastern U.S.
879 cold season severe weather environments, *Weather and Forecasting*,
880 <https://doi.org/10.1175/WAF-D-14-00105.1>, 2015.

881 Dong, X., Fu, J. S., Huang, K., Tong, D., and Zhuang, G.: Model development of dust emission
882 and heterogeneous chemistry within the Community Multiscale Air Quality modeling system
883 and its application over East Asia, *Atmos. Chem. Phys.*, 16, 8157–8180,
884 <https://doi.org/10.5194/acp-16-8157-2016>, 2016.

885 Eder, B. and Yu, S.: A performance evaluation of the 2004 release of Models-3 CMAQ, *Atmos.*
886 *Environ.*, 40(26):4811–4824, 2006.

887 Emery, C., Liu, Z., Russell, A. G., Odman, M. T., Yarwood, G., and Kumar, N.:
888 Recommendations on statistics and benchmarks to assess photochemical model performance, J.
889 Air Waste Manage. Assoc., 67:5, 582-598, doi:10.1080/10962247.2016.1265027, 2017.

890 Emmons, L. K., Edwards, D. P., Deeter, M. N., Gille, J. C., Campos, T., Nédélec, P., Novelli, P.,
891 and Sachse, G.: Measurements of Pollution In The Troposphere (MOPITT) validation through
892 2006, Atmos. Chem. Phys., 9, 1795–1803, <https://doi.org/10.5194/acp-9-1795-2009>, 2009.

893 Gan, C.-M., Pleim, J., Mathur, R., Hogrefe, C., Long, C. N., Xing, J., Wong, D., Gilliam, R., and
894 Wei, C.: Assessment of long-term WRF–CMAQ simulations for understanding direct aerosol
895 effects on radiation "brightening" in the United States, Atmos. Chem. Phys., 15, 12193–12209,
896 <https://doi.org/10.5194/acp-15-12193-2015>, 2015a.

897 Gan, C.-M., Binkowski, F., Pleim, J., Xing, J., Wong, D., Mathur, R., and Gilliam, R.:
898 Assessment of the aerosol optics component of the coupled WRF–CMAQ model using CARES
899 field campaign data and a single column model, Atmos. Environ., 115, 670-682, 2015b.

900 Gantt, B., He, J., Zhang, X., Zhang, Y., and Nenes, A.: Incorporation of advanced aerosol
901 activation treatments into CESM/CAM5: model evaluation and impacts on aerosol indirect
902 effects, Atmos. Chem. Phys., 14, 7485–7497, <https://doi.org/10.5194/acp-14-7485-2014>, 2014.

903 Gantt, B., Sarwar, G., Xing, J., Simon, H., Schwede, D., Hutzell, W. T., Mathur, R., and Saiz-
904 Lopez, A.: The impact of iodide-mediated ozone deposition and halogen chemistry on surface
905 ozone concentrations across the continental United States, Environ. Sci. Technol., 51 (3), 1458-
906 1466, 2017.

907 Ghan, S. J., Laulainen, N. S., Easter, R. C., Wagener, R., Nemesure, S., Chapman, E. G., Zhang,
908 Y., and Leung, L. R.: Evaluation of aerosol direct radiative forcing in MIRAGE, J. Geophys.
909 Res., 106, 5295–5316, 2001.

910 Glotfelty, T., He, J., and Zhang, Y.: Impact of future climate policy scenarios on air quality and
911 aerosol-cloud interactions using an advanced version of CESM/CAM5: Part I. model evaluation
912 for the current decadal simulations, Atmos. Environ., 152, 222-239, 2017.

913 Grell, G. A., Peckham, S. E., Schmitz, R., McKenn, S. A., Frost, G., Skamarock, W. C., and
914 Eder, B.: Fully Coupled "Online" chemistry within the WRF Model, Atmos. Environ., 39, 6957–
915 6975, 2005.

916 Grell, G. A. and Baklanov, A.: Integrated modelling for forecasting weather and air quality: A
917 call for fully coupled approaches, Atmos. Environ., 45, 38, 6845–6851, 2011.

918 He, J. and Zhang, Y.: Improvement and further development in CESM/CAM5: Gasphase
919 chemistry and inorganic aerosol treatments, Atmos. Chem. Phys., 14, 9171-9200,
920 <http://dx.doi.org/10.5194/acp-14-9171-2014>, 2014.

921 Heald, C. L., Jacob, D. J., Fiore, A. M., Emmons, L. K., Gille, J. C., Deeter, M. N., Warner, J.,
922 Edwards, D. P., Crawford, J. H., Hamlin, A. J., Sachse, G. W., Browell, E. V., Avery, M. A.,
923 Vay, S. A., Westberg, D. J., Blake, D. R., Singh, H. B., Sandholm, S. T., Talbot, R. W., and
924 Fuelberg, H. E.: Asian outflow and trans-Pacific transport of carbon monoxide and ozone

925 pollution: An integrated satellite, aircraft, and model perspective, *J. Geophys. Res.*, 108(D24),
926 4804, doi:10.1029/2003JD003507, 2003.

927 Herwehe, J. A., Otte, T. L., Mathur, R., and Rao, S. T.: Diagnostic analysis of ozone
928 concentrations simulated by two regional-scale air quality models, *Atmos. Environ.*, 45, 5957–
929 5969, 2011.

930 Hogrefe, C., Pouliot, G., Wong, D., Torian, A., Roselle, S., Pleim, J., and Mathur, R.: Annual
931 application and evaluation of the online coupled WRF–CMAQ system over North America
932 under AQMEII phase 2, *Atmos. Environ.*, 115, 683–694, 2015.

933 Hong, C., Zhang, Q., Zhang, Y., Tang, Y., Tong, D., and He, K.: Multi-year downscaling
934 application of two-way coupled WRF v3.4 and CMAQ v5.0.2 over east Asia for regional climate
935 and air quality modeling: model evaluation and aerosol direct effects, *Geosci. Model Dev.*, 10,
936 2447–2470, <https://doi.org/10.5194/gmd-10-2447-2017>, 2017.

937 Hong, C.-P., Zhang, Q., Zhang, Y., Davis, S. J., Zhang, X., Tong, D., Guan, D., Liu, Z., and He,
938 K.-B.: Weakened aerosol radiative effects may mitigate the climate penalty on Chinese air
939 quality, *Nature Climate Change*, in press, 2020.

940 Iacono, M. J., Delamere, J. S., Mlawer, E. J., Shephard, M. W., Clough, S. A., and Collins, W.
941 D.: Radiative forcing by long-lived greenhouse gases: Calculations with the AER radiative
942 transfer models, *J. Geophys. Res. Atmos.*, 113, D13103, <https://doi.org/10.1029/2008JD009944>,
943 2008.

944 IPCC: Global warming of 1.5°C, An IPCC Special Report on the impacts of global warming of
945 1.5°C above pre-industrial levels and related global greenhouse gas emission pathways, in the
946 context of strengthening the global response to the threat of climate change, sustainable
947 development, and efforts to eradicate poverty edited by Masson-Delmotte, V., Zhai, P., Pörtner,
948 H. O., Roberts, D., Skea, J., Shukla, P. R., Pirani, A., Moufouma-Okia, W., Péan, C., Pidcock,
949 R., Connors, S., Matthews, J. B. R., Chen, Y., Zhou, X., Gomis, M. I., Lonnoy, E., Maycock, T.,
950 Tignor, M., and Waterfield, T., 2018.

951 Jacobson, M. Z., Lu, R., Turco, R. P., and Toon, O. B.: Development and application of a new
952 air pollution modeling system. Part I: Gas-phase simulations, *Atmos. Environ.*, 30B, 1939–1963,
953 1996.

954 Jacobson, M. Z.: GATOR-GCMM: A global- through urban-scale air pollution and weather
955 forecast model 1. Model design and treatment of subgrid soil, vegetation, roads, rooftops, water,
956 sea, ice, and snow, *J. Geophys. Res.*, 106, 5385–5401, 2001.

957 Jung, J., Souri, A. H., Wong, D. C., Lee, S., Jeon, W., Kim, J., and Choi, Y.: The impact of the
958 direct effect of aerosols on meteorology and air quality using aerosol optical depth assimilation
959 during the KORUS - AQ campaign, *J. Geophys. Res. Atmos.*, 124, 8303–8319,
960 <https://doi.org/10.1029/2019JD030641>, 2019.

961 Kain, J. S.: The Kain-Fritsch convective parameterization: An update, *J. Appl. Meteorol.*, 43,
962 170–181, [https://doi.org/10.1175/1520-0450\(2004\)043<0170:TKCPAU>2.0.CO;2](https://doi.org/10.1175/1520-0450(2004)043<0170:TKCPAU>2.0.CO;2), 2004.

963 Karydis, V. A., Tsimpidi, A. P., and Pandis, S. N.: Evaluation of a three-dimensional chemical
964 transport model (PMCAMx) in the eastern United States for all four seasons, *J. Geophys. Res.*,
965 112, D14211, doi:10.1029/2006JD007890, 2007.

966 Kaufman, Y. J., Smirnov, A., Holben, B., and Dubovik, O.: Baseline maritime aerosol
967 methodology to derive the optical thickness and scattering properties, *Geophys. Res. Lett.*, 28,
968 3251, doi:10.1029/2001GL013312, 2001.

969 Kelly, J., Koplitz, S., Baker, K., Holder, A., Pye, H., Murphy, B., Bash, J., Henderson, B.,
970 Possiel, N., Simon, H., Eyth, A., Jang, C., Phillips, S., and Timin, B.: Assessing PM_{2.5} model
971 performance for the conterminous U.S. with comparison to model performance statistics from
972 2007-2015, *Atmos. Environ.*, 214, <https://doi.org/10.1016/j.atmosenv.2019.116872>, 2019.

973 Kukkonen, J., Olsson, T., Schultz, D. M., Baklanov, A., Klein, T., Miranda, A. I., Monteiro, A.,
974 Hirtl, M., Tarvainen, V., Boy, M., Peuch, V.-H., Poupkou, A., Kioutsioukis, I., Finardi, S.,
975 Sofiev, M., Sokhi, R., Lehtinen, K. E. J., Karatzas, K., San José, R., Astitha, M., Kallos, G.,
976 Schaap, M., Reimer, E., Jakobs, H., and Eben, K.: A review of operational, regional-scale,
977 chemical weather forecasting models in Europe, *Atmos. Chem. Phys.*, 12, 1–87,
978 doi:10.5194/acp-12-1-2012, 2012.

979 Li, P., Wang, L., Guo, P., Yu, S., Mehmood, K., Wang, S., Liu, W., Seinfeld, J. H., Zhang, Y.,
980 Wong, D., Alapaty, K., Pleim, J., and Mathur, R.: High reduction of ozone and particulate matter
981 during the 2016 G-20 summit in Hangzhou by forced emission controls of industry and traffic,
982 *Environ. Chem. Lett.*, 15:709–715, doi:10.1007/s10311-017-0642-2, 2017.

983 Lin, M., Holloway, T., Carmichael, G. R., and Fiore, A. M.: Quantifying pollution inflow and
984 outflow over East Asia in spring with regional and global models, *Atmos. Chem. Phys.*, 10,
985 4221–4239, <https://doi.org/10.5194/acp-10-4221-2010>, 2010.

986 Liu, X.-H., Zhang, Y., Xing, J., Zhang, Q., Wang, K., Streets, D. G., Jang, C. J., Wang, W.-X.,
987 and Hao, J. M.: Understanding of regional air pollution over China using CMAQ:- Part II.
988 Process analysis and ozone sensitivity to precursor emissions, *Atmos. Environ.*, 44(20), 3719–
989 3727, 2010.

990 Lorente, A., Folkert Boersma, K., Yu, H., Dörner, S., Hilboll, A., Richter, A., Liu, M., Lamsal,
991 L. N., Barkley, M., De Smedt, I., Van Roozendaal, M., Wang, Y., Wagner, T., Beirle, S., Lin, J.-
992 T., Krotkov, N., Stammes, P., Wang, P., Eskes, H. J., and Kröl, M.: Structural uncertainty in air
993 mass factor calculation for NO₂ and HCHO satellite retrievals, *Atmos. Meas. Tech.*, 10, 759–
994 782, <https://doi.org/10.5194/amt-10-759-2017>, 2017.

995 Ma, P.-L., Rasch, P. J., Fast, J. D., Easter, R. C., Gustafson Jr., W. I., Liu, X., Ghan, S. J., and
996 Singh, B.: Assessing the CAM5 physics suite in the WRF-Chem model: implementation,
997 resolution sensitivity, and a first evaluation for a regional case study, *Geosci. Model Dev.*, 7,
998 755–778, <https://doi.org/10.5194/gmd-7-755-2014>, 2014.

999 Makar, P., A., Gong, W., Hogrefe, C., Zhang, Y., Curci, G., Žabkar, R., Milbrandt, J., Im, U.,
1000 Balzarini, A., Baró, R., Bianconi, R., Cheung, P., Forkel, R., Gravel, S., Hirtl, M., Honzak, L.,
1001 Hou, A., Jiménez-Guerrero, P., Langer, M., Moran, M. B., Pabla, B., Pérez, J. L., Pirovano, G.,

1002 San José, R., Tuccella, P., Werhahn, J., Zhang, J., and Galmarini, S.: Feedbacks between air
1003 pollution and weather, Part 2: Effects on chemistry, *Atmos. Environ.*, 115, 499-526, 2015.

1004 Mathur, R., Xiu, A., Coats, C., Alapaty, K., Shankar, U., and Hanna, A.: Development of an air
1005 quality modeling system with integrated meteorology, chemistry, and emissions, *Proc.*
1006 *Measurement of Toxic and Related Air Pollutants*, AWMA, Cary, NC, September, 1998.

1007 Mathur, R., Xing, J., Gilliam, R., Sarwar, G., Hogrefe, C., Pleim, J., Pouliot, G., Roselle, S.,
1008 Spero, T. L., Wong, D. C., and Young, J.: Extending the Community Multiscale Air Quality
1009 (CMAQ) modeling system to hemispheric scales: overview of process considerations and initial
1010 applications, *Atmos. Chem. Phys.*, 17, 12449-12474, 2017.

1011 Matsui, H., Koike, M., Kondo, Y., Takegawa, N., Kita, K., Miyazaki, Y., Hu, M., Chang, S.-Y.,
1012 Blake, D. R., Fast, J. D., Zaveri, R. A., Streets, D. G., Zhang, Q. and Zhu, T.: Spatial and
1013 temporal variations of aerosols around Beijing in summer 2006: Model evaluation and source
1014 apportionment, *J. Geophys. Res.*, 114, D00G13, doi:10.1029/2008JD010906, 2009.

1015 Mebust, M. R., Eder, B. K., Binkowski, F. S., and Roselle, S. J.: Models-3 Community
1016 Multiscale Air Quality (CMAQ) model aerosol component: 2. Model evaluation, *J. Geophys.*
1017 *Res.*, 108(D6), 4184, doi:10.1029/2001JD001410, 2003.

1018 Mehmood, K., Wu, Y., Wang, L., Yu, S., Li, P., Chen, X., Li, Z., Zhang, Y., Li, M., Liu, W.,
1019 Wang, Y., Liu, Z., Zhu, Y., Rosenfeld, D., and Seinfeld, J. H.: Relative effects of open biomass
1020 burning and open crop straw burning on haze formation over central and eastern China:
1021 modeling study driven by constrained emissions, *Atmos. Chem. Phys.*, 20, 2419–2443,
1022 <https://doi.org/10.5194/acp-20-2419-2020>, 2020.

1023 Morrison, H., Thompson, G., and Tatarskii, V.: Impact of cloud microphysics on the
1024 development of trailing stratiform precipitation in a simulated squall line: Comparison of one-
1025 and two-moment schemes, *Mon. Weather Rev.*, 137, 991–1007,
1026 <https://doi.org/10.1175/2008MWR2556.1>, 2009.

1027 Penrod, A., Zhang, Y., Wang, K., Wu, S.-Y., and Leung, R. L.: Impacts of future climate and
1028 emission changes on US air quality, *Atmos. Environ.*, 89, 533-547,
1029 doi:10.1016/j.atmosenv.2014.01.001, 2014.

1030 Pleim, J. E.: A combined local and nonlocal closure model for the atmospheric boundary layer.
1031 Part I: Model description and testing, *J. Appl. Meteorol. Clim.*,
1032 <https://doi.org/10.1175/JAM2539.1>, 2007.

1033 Pleim, J., Young, J., Wong, D., Gilliam, R., Otte, T., and Mathur, R.: Two-way coupled
1034 meteorology and air quality modeling, in *Air Pollution Modeling and its Application*, edited by
1035 C. Borrego and A. I. Miranda, XIX, NATO Science for Peace and Security Series, Series C:
1036 *Environmental Security*, Springer, Dordrecht, 2008.

1037 Pleim, J. E. and Gilliam, R.: An indirect data assimilation scheme for deep soil temperature in
1038 the Pleim–Xiu land surface model, *J. Appl. Meteorol. Clim.*, 48, 1362-1376, 2009.

1039 Pye, H. O. T., Murphy, B. N., Xu, L., Ng, N. L., Carlton, A. G., Guo, H., Weber, R., Vasilakos,
1040 P., Appel, K. W., Budisulistiorini, S. H., Surratt, J. D., Nenes, A., Hu, W., Jimenez, J. L.,
1041 Isaacman-VanWertz, G., Misztal, P. K., and Goldstein, A. H.: On the implications of aerosol
1042 liquid water and phase separation for organic aerosol mass, *Atmos. Chem. Phys.*, 17, 343–369,
1043 doi:10.5194/acp-17-343-2017, 2017.

1044 Pye, H. O. T., Nenes, A., Alexander, B., Ault, A. P., Barth, M. C., Clegg, S. L., Collett Jr., J. L.,
1045 Fahey, K. M., Hennigan, C. J., Herrmann, H., Kanakidou, M., Kelly, J. T., Ku, I.-T., McNeill, V.
1046 F., Riemer, N., Schaefer, T., Shi, G., Tilgner, A., Walker, J. T., Wang, T., Weber, R., Xing, J.,
1047 Zaveri, R. A., and Zuend, A.: The acidity of atmospheric particles and clouds, *Atmos. Chem.*
1048 *Phys.*, 20, 4809–4888, <https://doi.org/10.5194/acp-20-4809-2020>, 2020.

1049 Remer, L. A., Kaufman, Y. J., Tarré, D., Mattoo, S., Chu, D. A., Martins, J. V., Li, R. R.,
1050 Ichoku, C., Levy, R. C., and Kleidman, R. G.: The MODIS aerosol algorithm, products, and
1051 validation, *J. Atmos. Sci.*, 62, 947-973, 2005.

1052 Roy, B., Pouliot, G. A., Gilliland, A., Pierce, T., Howard, S., Bhave, P. V., and Benjey, W.:
1053 Refining fire emissions for air quality modeling with remotely sensed fire counts: A wildfire case
1054 study, *Atmos. Environ.*, 41(3), 655-665, doi:10.1016/j.atmosenv.2006.08.037, 2007.

1055 San Joaquin Valley Air Pollution Control District: 2018 Plan for the 1997, 2006, and 2012 PM_{2.5}
1056 Standards, November 15, 2018, <https://www.valleyair.org/pmplans>, 2018.

1057 Sarwar, G., Luecken, D., Yarwood, G., Whitten, G. Z., and Carter, W. P. L.: Impact of an
1058 updated carbon bond mechanism on predictions from the CMAQ modeling system: Preliminary
1059 assessment, *J. Appl. Meteor. Clim.*, 47, 3e14, 2008.

1060 Sarwar, G., Gantt, B., Schwede, D., Foley, K., Mathur, R., and Saiz-Lopez, A.: Impact of
1061 enhanced ozone deposition and halogen chemistry on tropospheric ozone over the Northern
1062 Hemisphere, *Environ. Sci. Technol.*, 49 (15), 9203-9211, 2015.

1063 Scheffe, R. D., Strum, M., Phillips, S. B., Thurman, J., Eyth, A., Fudge, S., Morris, M., Palma,
1064 T., and Cook, R.: Hybrid modeling approach to estimate exposures of hazardous air pollutants
1065 (HAPs) for the National Air Toxics Assessment (NATA), *Environ. Sci. Technol.*, 2016, 50(22),
1066 12356–12364, doi:10.1021/acs.est.6b04752, 2016.

1067 Schwede, D., Pouliot, G. A., and Pierce, T.: Changes to the biogenic emissions inventory system
1068 version 3 (BEIS3), in: *Proceedings of the 4th CMAS Models-3 Users' Conference*, Chapel Hill,
1069 NC, 26–28 September, 2005.

1070 Sekiguchi, A., Shimadera, H., and Kondo, A.: Impact of aerosol direct effect on wintertime
1071 PM_{2.5} simulated by an online coupled meteorology-air quality model over East Asia, *Aerosol.*
1072 *Air Qual. Res.*, 18, 1068–1079, 2018.

1073 Solazzo, E., Hogrefe, C., Colette, A., Garcia-Vivanco, M., and Galmarini, S.: Advanced error
1074 diagnostics of the CMAQ and Chimere modelling systems within the AQMEII3 model
1075 evaluation framework, *Atmos. Chem. Phys.*, 17, 10435-10465, 2017.

1076 [Stavrakou, T., Müller, J.-F., De Smedt, I., Van Roozendael, M., van der Werf, G. R., Giglio, L.,](#)
1077 [and Guenther, A.: Global emissions of non-methane hydrocarbons deduced from SCIAMACHY](#)
1078 [formaldehyde columns through 2003–2006, Atmos. Chem. Phys., 9, 3663–3679,](#)
1079 [doi:10.5194/acp-9-3663-2009, 2009.](#)

1080 [U.S. EPA: Our nation’s air status and trends through 2010, EPA-454/R-12-001, February 2012,](#)
1081 [https://www.epa.gov/sites/default/files/2017-11/documents/trends_brochure_2010.pdf, 2012,](#)

1082 U.S. EPA: Policy assessment for the review of the National Ambient Air Quality Standards for
1083 particulate matter, EPA-452/R-20-002, January 2020,
1084 [https://www.epa.gov/sites/production/files/2020-](#)
1085 [01/documents/final_policy_assessment_for_the_review_of_the_pm_naaqs_01-2020.pdf, 2020.](#)

1086 Vasilakos, P., Russell, A., Weber, R., and Nenes, A.: Understanding nitrate formation in a world
1087 with less sulfate. Atmos. Chem. Phys. 18, 12765-12775, 2018.

1088 Wang, K. and Zhang, Y.: Application, evaluation, and process analysis of U.S. EPA’s 2002
1089 multiple-pollutant air quality modeling platform, Atmospheric and Climate Sciences, 2, 254-289,
1090 2012.

1091 Wang, K. and Zhang, Y.: 3-D agricultural air quality modeling: Impacts of NH₃/H₂S gas-phase
1092 reactions and bi-directional exchange of NH₃, Atmos. Environ., 98, 554-570, doi:
1093 10.1016/j.atmosenv.2014.09.010, 2014.

1094 Wang, K., Zhang, Y., Jang, C., Phillips, S., and Wang, B.: Modeling intercontinental air
1095 pollution transport over the trans-Pacific region in 2001 using the Community Multiscale Air
1096 Quality modeling system, J. Geophys. Res., 114, D04307, doi:10.1029/2008JD010807, 2009.

1097 Wang, K., Zhang, Y., Nenes, A., and Fountoukis, C.: Implementation of dust emission and
1098 chemistry into the Community Multiscale Air Quality modeling system and initial application to
1099 an Asian dust storm episode, Atmos. Chem. Phys., 12, 10209–10237,
1100 [https://doi.org/10.5194/acp-12-10209-2012, 2012.](#)

1101 Wang, J., Wang, S., Jiang, J., Ding, A., Zheng, M., Zhao, B., Wong, C.-D., Zhou, W., Zheng, G.,
1102 Wang, L., Pleim, J., and Hao, J.: Impact of aerosol–meteorology interactions on fine particle
1103 pollution during China’s severe haze episode in January 2013, Environ. Res. Lett., 9,
1104 doi:10.1088/1748-9326/9/9/094002, 2014.

1105 Wang, K., Zhang, Y., Yahya, K., Wu, S.-Y., and Grell, G.: Implementation and initial
1106 application of new chemistry-aerosol options in WRF/Chem for simulating secondary organic
1107 aerosols and aerosol indirect effects for regional air quality, Atmos. Environ., 115, 716-732,
1108 doi:10.1016/j.atmosenv.2014.12.007, 2015a.

1109 Wang, K., Yahya, K., Zhang, Y., Hogrefe, C., Pouliot, G., Knote, C., Hodzic, A., Jose, R. S.,
1110 Perez, J. L., Jiménez-Guerrero, P., Baro, R., Makar, P., and Bennartz, R.: A multi-model
1111 assessment for the 2006 and 2010 simulations under the Air Quality Model Evaluation
1112 International Initiative (AQMEII) Phase 2 over North America: Part II. Evaluation of column
1113 variable predictions using satellite data, Atmos. Environ., 115, 1–17,
1114 10.1016/j.atmosenv.2014.07.044, 2015b.

Formatted: Space After: 10 pt

Formatted: Don't adjust right indent when grid is defined, Don't adjust space between Latin and Asian text, Don't adjust space between Asian text and numbers

Formatted: Font color: Auto, Pattern: Clear

1115 Wang, K., Zhang, Y., and Yahya, K.: Decadal application of WRF/Chem over the continental
1116 U.S.: Simulation design, sensitivity simulations, and climatological model evaluation, *Atmos.*
1117 *Environ.*, 118331, doi: 10.1016/j.atmosenv.2021.118331, 2021.

1118 West, J. J., Ansari, A. S., and Pandis, S. N.: Marginal PM_{2.5}: Nonlinear aerosol mass response to
1119 sulfate reductions in the Eastern United States, *J. Air Waste Manage. Assoc.*, 49, 1415-1424,
1120 <https://doi.org/10.1080/10473289.1999.10463973>, 1999.

1121 Wiedinmyer, C., Quayle, B., Geron, C., Belote, A., McKenzie, D., Zhang, X., O'Neill, S., and
1122 Wynne, K. K.: Estimating emissions from fires in North America for air quality modeling,
1123 *Atmos. Environ.*, 40(19): 3419–32, doi:10.1016/j.atmosenv.2006.02.010, 2006.

1124 Wielicki, B. A., Barkstrom, B. R., Harrison, E. F., Lee III, R. B., Smith, G. L., and Cooper, J. E.:
1125 Clouds and the Earth's Radiant Energy System (CERES): An earth observing system
1126 experiment, *B. Am. Meteorol. Soc.*, 77, 853–868, 1996.

1127 Wilczak, J. M., Djalalova, I., McKeen, S., Bianco, L., Bao, J.-W., Grell, G., Peckham, S.,
1128 Mathur, R., McQueen, J., and Lee, P.: Analysis of regional meteorology and surface ozone during
1129 the TexAQS II field program and an evaluation of the NMM-CMAQ and WRF-Chem air quality
1130 models, *J. Geophys. Res.*, 114, D00F14, 2009.

1131 Wong, D. C., Pleim, J., Mathur, R., Binkowski, F., Otte, T., Gilliam, R., Pouliot, G., Xiu, A.,
1132 Young, J. O., and Kang, D.: WRF-CMAQ two-way coupled system with aerosol feedback:
1133 Software development and preliminary results, *Geosci. Model Dev.*, 5, 299–312,
1134 <https://doi.org/10.5194/gmd-5-299-2012>, 2012.

1135 Xing, J., Mathur, R., Pleim, J., Hogrefe, C., Gan, C.-M., Wong, D. C., Wei, C., and Wang, J.: Air
1136 pollution and climate response to aerosol direct radiative effects: A modeling study of decadal
1137 trends across the northern hemisphere, *J. Geophys. Res. Atmos.*, 120, 12,221–12,236,
1138 doi:10.1002/2015JD023933, 2015a.

1139 Xing, J., Mathur, R., Pleim, J., Hogrefe, C., Gan, C.-M., Wong, D. C., and Wei, C.: Can a
1140 coupled meteorology–chemistry model reproduce the historical trend in aerosol direct radiative
1141 effects over the Northern Hemisphere?, *Atmos. Chem. Phys.*, 15, 9997–10018,
1142 <https://doi.org/10.5194/acp-15-9997-2015>, 2015b.

1143 Xing, J., Wang, J., Mathur, R., Pleim, J., Wang, S., Hogrefe, C., Gan, C.-M., Wong, D., and Hao,
1144 J.: Unexpected benefits of reducing aerosol cooling effects, *Environ. Sci. Technol.*, 50, 7527–
1145 7534, <https://doi.org/10.1021/acs.est.6b00767>, 2016.

1146 Xing, J., Wang, J., Mathur, R., Wang, S., Sarwar, G., Pleim, J., Hogrefe, C., Zhang, Y., Jiang, J.,
1147 Wong, D. C., and Hao, J.: Impacts of aerosol direct effects on tropospheric ozone through
1148 changes in atmospheric dynamics and photolysis rates, *Atmos. Chem. Phys.*, 17, 9869–9883,
1149 <https://doi.org/10.5194/acp-17-9869-2017>, 2017.

1150 Xiu, A. and Pleim, J. E.: Development of a land surface model. Part I: Application in a
1151 mesoscale meteorological model, *J. Appl. Meteorol.*, 40, 192–209, [https://doi.org/10.1175/1520-0450\(2001\)040<0192:doalsm>2.0.co;2](https://doi.org/10.1175/1520-0450(2001)040<0192:doalsm>2.0.co;2), 2001.

1153 Yahya, K., Wang, K., Gudoshava, M., Glotfelty, T., and Zhang, Y.: Application of WRF/Chem
 1154 over North America under the AQMEII Phase 2. Part I. Comprehensive evaluation of 2006
 1155 simulation, *Atmos. Environ.*, 115, 733-755, doi:10.1016/j.atmosenv.2014.08.063, 2015a.

1156 Yahya, K., Wang, K., Zhang, Y., and Kleindienst, T. E.: Application of WRF/Chem over North
 1157 America under the AQMEII Phase 2 – Part 2: Evaluation of 2010 application and responses of
 1158 air quality and meteorology–chemistry interactions to changes in emissions and meteorology
 1159 from 2006 to 2010, *Geosci. Model Dev.*, 8, 2095–2117, [https://doi.org/10.5194/gmd-8-2095-](https://doi.org/10.5194/gmd-8-2095-2015)
 1160 2015, 2015b.

1161 Yahya, K., Wang, K., Campbell, P., Glotfelty, T., He, J., and Zhang, Y.: Decadal evaluation of
 1162 regional climate, air quality, and their interactions over the continental US and their interactions
 1163 using WRF/Chem version 3.6.1, *Geosci. Model Dev.*, 9, 671–695, [https://doi.org/10.5194/gmd-](https://doi.org/10.5194/gmd-9-671-2016)
 1164 9-671-2016, 2016.

1165 Yarwood, G., Rao, S., Yocke, M., and Whitten, G. Z.: Final Report–Updates to the Carbon Bond
 1166 Chemical Mechanism: CB05, Rep.RT-04-00675, Yocke and Co., Novato, Calif., 246 pp., 2005.

1167 Yoo, J.-W., Jeon, W., Park, S.-Y., Park, C., Jung, J., Lee, S.-H., and Lee, H. W.: Investigating
 1168 the regional difference of aerosol feedback effects over South Korea using the WRF-CMAQ
 1169 two-way coupled modeling system, *Atmos. Environ.*, 218, 116968, 2019.

1170 Yu, S., Eder, B., Dennis, R., Chu, S., and Schwartz, S.: New unbiased symmetric metrics for
 1171 evaluation of air quality models, *Atmos. Sci. Lett.*, 7, 26-34, 2006.

1172 Yu, S. C., Mathur, R., Schere, K., Kang, D., Pleim, J., and Otte, T. L.: A detailed evaluation of
 1173 the Eta-CMAQ forecast model performance for O₃, its related precursors, and meteorological
 1174 parameters during the 2004 ICARTT Study, *J. Geophys. Res.*, 112, D12S14,
 1175 doi:10.1029/2006JD007715, 2007.

1176 Yu, S. C., Mathur, R., Pleim, J., Wong, D., Carlton, A. G., Roselle, S., and Rao, S. T.:
 1177 Simulation of the indirect radiative forcing of climate due to aerosols by the two-way coupled
 1178 WRF-CMAQ over the eastern United States, in *Air Pollution Modeling and its Applications*,
 1179 edited by D. G. Steyn and S. T. Castell, XXI, Springer Netherlands, Netherlands, C(96), 579–
 1180 583, 2011.

1181 Yu, S., Mathur, R., Pleim, J., Wong, D., Gilliam, R., Alapaty, K., Zhao, C., and Liu, X.: Aerosol
 1182 indirect effect on the grid-scale clouds in the two-way coupled WRF–CMAQ: Model
 1183 description, development, evaluation and regional analysis, *Atmos. Chem. Phys.*, 14, 11247–
 1184 11285, <https://doi.org/10.5194/acp-14-11247-2014>, 2014.

1185 Yu, S., Li, P., Wang, L., Wu, Y., Wang, S., Liu, W., Zhu, T., Zhang, Y., Hu, M., Alapaty, K.,
 1186 Wong, D., Pleim, J., Mathur, R., Rosenfeld, D., and Seinfeld, J.: Mitigation of severe urban haze
 1187 pollution by a precision air pollution control approach, *Scientific Reports*, 8:8151,
 1188 doi:10.1038/s41598-018-26344-1, 2018.

1189 Yu, X.-Y., Lee, T., Ayres, B., Kreidenweis, S. M., Malm, W., and Collett, J. L.: Loss of fine
 1190 particle ammonium from denuded nylon filters, *Atmos. Environ.*, 40, 4797-4807, 2006.

1191 Zender, C. S., H. Bian, and D. Newman: Mineral Dust Entrainment and Deposition (DEAD)
1192 model: Description and 1990s dust climatology, *J. Geophys. Res.*, 108, 4416,
1193 doi:10.1029/2002JD002775, 2003.

1194 Zhang, Y.: Online coupled meteorology and chemistry models: History, current status, and
1195 outlook, *Atmos. Chem. Phys.*, 8, 2895-2932, doi:10.5194/acp-8-2895-2008, 2008.

1196 Zhang, Y. and Wang, Y.: Climate-driven ground-level ozone extreme in the fall over the
1197 Southeast United States, *P. Natl. Acad. Sci. USA*, 113, 10025–10030,
1198 <https://doi.org/10.1073/pnas.1602563113>, 2016.

1199 Zhang, Y. and Wang, K.: Project 3 - Air quality and climate modeling: Multi-model application,
1200 evaluation, intercomparison, and ensemble over the U.S., poster presentation at the Air Climate
1201 Energy (ACE) Centers Meeting, Pittsburgh, PA, June 18-19, 2019.

1202 Zhang, K. M., Knipping, E. M., Wexler, A. S., Bhawe, P. V., and Tonnesen, G. S.: Size
1203 distribution of sea-salt emissions as a function of relative humidity, *Atmos. Environ.*, 39, 3373-
1204 3379, 2005.

1205 Zhang, Y., Liu, P., Pun, B., and Seigneur, C.: A comprehensive performance evaluation of MM5-
1206 CMAQ for the summer 1999 Southern Oxidants Study episode, Part-I. Evaluation protocols,
1207 databases and meteorological predictions, *Atmos. Environ.*, 40, 4825-4838,
1208 doi:10.1016/j.atmosenv.2005.12.043, 2006.

1209 Zhang, Y., Vijayaraghavan, K., Wen, X.-Y., Snell, H. E., and Jacobson, M. Z.: Probing into
1210 regional ozone and particulate matter pollution in the United States: 1. A 1-year CMAQ
1211 simulation and evaluation using surface and satellite data, *J. Geophys. Res.*, 114, D22304,
1212 doi:10.1029/2009JD011898, 2009a.

1213 Zhang, Y., Wen, X.-Y., Wang, K., Vijayaraghavan, K., and Jacobson, M. Z.: Probing into
1214 regional ozone and particulate matter pollution in the United States: 2. An examination of
1215 formation mechanisms through a process analysis technique and sensitivity study, *J. Geophys.*
1216 *Res.*, 114, D22305, doi:10.1029/2009JD011900, 2009b.

1217 Zhang, Y., Wen, X.-Y., and Jang C. J.: Simulating chemistry-aerosol-cloud-radiation-climate
1218 feedbacks over the continental US using the online-coupled Weather Research Forecasting
1219 Model with chemistry (WRF/Chem), *Atmos. Environ.*, 44(29), 3568-3582, doi:
1220 10.1016/j.atmosenv.2010.05.056, 2010.

1221 Zhang, Y., Sartelet, K., Zhu, S., Wang, W., Wu, S.-Y., Zhang, X., Wang, K., Tran, P., Seigneur,
1222 C., and Wang, Z.-F.: Application of WRF/Chem-MADRID and WRF/Polyphemus in Europe –
1223 Part 2: Evaluation of chemical concentrations and sensitivity simulations, *Atmos. Chem. Phys.*,
1224 13, 6845–6875, <https://doi.org/10.5194/acp-13-6845-2013>, 2013.

1225 Zhang, Y., Chen, Y., Fan, J., and Leung, L. R.: Application of an online-coupled regional
1226 climate model, WRF-CAM5, over East Asia for examination of ice nucleation schemes: Part II.
1227 Sensitivity to ice nucleation parameterizations and dust emissions, *Climate*, 3(3), 753-774,
1228 doi:10.3390/cli3030753, 2015a.

1229 Zhang, Y., Zhang, X., Wang, K., He, J., Leung, L. R., Fan, J.-W., and Nenes, A.: Incorporating
1230 an advanced aerosol activation parameterization into WRF-CAM5: Model evaluation and
1231 parameterization intercomparison, *J. Geophys. Res.*, 120 (14), doi:10.1002/2014JD023051,
1232 2015b.

1233 Zhang, Y., Zhang, X., Wang, L., Zhang, Q., Duan, F., and He, K.: Application of WRF/Chem
1234 over East Asia: Part I. Model evaluation and intercomparison with MM5/CMAQ, *Atmos.*
1235 *Environ.*, 124, 285–300, 2016a.

1236 Zhang, Y., Hong, C.-P., Yahya, K., Li, Q., Zhang, Q., and He, K.-B.: Comprehensive evaluation
1237 of multi-year real-time air quality forecasting using an online-coupled meteorology-chemistry
1238 model over southeastern United States, *Atmos. Environ.*, 138, 162-182,
1239 doi:10.1016/j.atmosenv.2016.05.006, 2016b.

1240 Zhang, Y., Wang, K., and He J.: Multi-year application of WRF-CAM5 over East Asia-Part II:
1241 Interannual variability, trend analysis, and aerosol indirect effects, *Atmos. Environ.*, 165, 222-
1242 239, 2017.

1243 Zhang, Y., Jena, C., Wang, K., Paton-Walsh, C., Guérette, E.-A., Utembe, S., Silver, J. D., and
1244 Keywood, M.: Multiscale applications of two online-coupled meteorology-chemistry models
1245 during recent field campaigns in Australia, Part I: Model description and WRF/Chem-ROMS
1246 evaluation using surface and satellite data and sensitivity to spatial grid resolutions, *Atmosphere*,
1247 10(4), 189, doi:10.3390/atmos10040189, 2019.

1248 Zheng, B., Zhang, Q., Zhang, Y., He, K. B., Wang, K., Zheng, G. J., Duan, F. K., Ma, Y. L., and
1249 Kimoto, T.: Heterogeneous chemistry: a mechanism missing in current models to explain
1250 secondary inorganic aerosol formation during the January 2013 haze episode in North China,
1251 *Atmos. Chem. Phys.*, 15, 2031–2049, <https://doi.org/10.5194/acp-15-2031-2015>, 2015.

Table 1. The 5-year average performance statistics for meteorological variables between two-way WRF-CMAQ and WRF-only simulations in winter, 2008-2012.

Variables	Datasets	Mean Obs	Two-way WRF-CMAQ				WRF-only					
			Mean Sim	R	MB	NMB (%)	RMSE	Mean Sim	R	MB	NMB (%)	RMSE
T2 (°C)	NCDC	7.5	8.6	0.97	1.1	14.9	1.6	8.6	0.97	1.2	15.8	1.6
RH2 (%)		72.9	75.1	0.79	2.2	3.0	6.3	75.0	0.79	2.1	2.8	6.3
WS10 (m s⁻¹)		3.93	4.50	0.4	0.57	14.6	1.17	4.50	0.4	0.58	14.6	1.17
WD10 (deg)		166.4	183.1	0.0	16.7	10.0	44.2	183.3	0.0	16.9	10.2	44.4
Precipitation (mm day⁻¹)	NCDC	1.54	2.25	0.46	0.71	46.3	1.94	2.26	0.47	0.72	47.0	1.94
	NADP	2.48	2.68	0.77	0.2	8.0	1.14	2.69	0.77	0.21	8.6	1.14
	GPCP	1.81	2.04	0.80	0.23	12.8	1.03	2.04	0.80	0.23	12.8	1.02
	PRISM	1.91	2.08	0.89	0.17	9.0	0.79	2.09	0.89	0.18	9.4	0.79
	TMPA	2.02	2.07	0.81	0.05	2.4	1.01	2.06	0.81	0.04	2.0	1.02
SWDOWN (W m⁻²)	CERES	108.5	119.8	0.99	11.3	10.4	13.7	128.0	0.98	19.5	17.9	22.2
GSW (W m⁻²)		87.1	94.6	0.99	7.5	8.6	10.1	101.3	0.98	14.1	16.2	17.1
GLW (W m⁻²)		278.9	278.0	0.99	-0.9	-0.3	5.9	272.7	0.99	-6.3	-2.2	8.6
OLR (W m⁻²)		222.3	226.2	0.99	4.0	1.8	5.1	227.0	0.99	4.7	2.1	5.8
SWCF (W m⁻²)		-26.6	-23.6	0.91	-3.0	-11.1	6.3	-19.2	0.85	-7.4	-27.8	10.6
LWCF (W m⁻²)		22.0	18.7	0.76	-3.3	-15.1	6.0	18.0	0.72	-4.1	-18.4	6.7
AOD		0.11	0.04	0.44	-0.06	-59.8	0.08	N/A	N/A	N/A	N/A	N/A
CF	0.66	0.59	0.87	-0.07	-10.4	0.1	N/A	N/A	N/A	N/A	N/A	
CDNC (cm⁻³)	MODIS	172.3	30.4	0.21	-141.9	-82.4	157.5	N/A	N/A	N/A	N/A	N/A
CWP (g m⁻²)		177.4	97.0	0.63	-80.4	-45.3	93.2	N/A	N/A	N/A	N/A	N/A
COT		16.9	3.3	0.74	-13.6	-80.8	14.2	N/A	N/A	N/A	N/A	N/A

*outputs of AOD, CF, CDNC, CWP, and COT are not available from WRF-only simulations

Table 2. The 5-year average performance statistics for meteorological variables between two-way WRF-CMAQ and WRF-only simulations in summer, 2008-2012.

Variables	Datasets	Mean Obs	Two-way WRF-CMAQ				WRF-only					
			Mean Sim	R	MB	NMB (%)	RMSE	Mean Sim	R	MB	NMB (%)	RMSE
T2 (°C)	NCDC	22.3	22.2	0.95	-1.1	-4.6	1.7	22.4	0.95	-0.9	-3.7	1.6
RH2 (%)		67.0	70.7	0.91	3.7	5.5	6.6	70.1	0.91	3.2	4.7	6.3
WS10 (m s ⁻¹)		3.19	3.57	0.36	0.38	11.8	0.99	3.61	0.35	0.42	13.1	1.01
WD10 (deg)		146.4	195.4	0.0	49.1	33.5	67.3	196.1	0.0	49.8	34.0	67.9
Precipitation (mm day ⁻¹)	NCDC	2.11	2.86	0.5	0.75	35.6	1.93	3.01	0.5	0.9	42.6	2.01
	NADP	2.82	2.99	0.83	0.17	5.9	0.87	3.14	0.83	0.32	11.2	0.93
	GPCP	2.55	2.78	0.80	0.23	9.0	1.19	2.86	0.80	0.30	11.9	1.21
	PRISM	2.35	2.55	0.89	0.20	8.4	0.69	2.65	0.89	0.30	12.9	0.73
	TMPA	2.70	2.83	0.80	0.13	4.8	1.27	2.89	0.81	0.19	6.8	1.27
SWDOWN (W m ⁻²)	CERES	254.7	298.3	0.84	43.6	17.1	46.6	314.1	0.73	59.4	23.3	62.8
GSW (W m ⁻²)		222.5	256.1	0.75	33.6	15.1	37.6	269.7	0.57	47.2	21.2	51.7
GLW (W m ⁻²)		372.2	358.8	0.98	-13.4	-3.6	15.3	355.4	0.98	-16.8	-4.5	18.7
OLR (W m ⁻²)		257.2	259.6	0.96	2.3	0.9	4.8	260.2	0.96	3.0	1.2	5.2
SWCF (W m ⁻²)		-55.1	-32.3	0.69	-22.8	-41.3	27.6	-24.0	0.50	-31.1	-56.4	36.2
LWCF (W m ⁻²)		26.1	17.5	0.85	-8.6	-33.0	9.8	17.1	0.87	-9.0	-34.6	10.0
AOD		0.20	0.07	0.67	-0.13	-67.8	0.14	N/A	N/A	N/A	N/A	N/A
CF	0.53	0.41	0.81	-0.12	-23.0	0.16	N/A	N/A	N/A	N/A	N/A	
CDNC (cm ⁻³)	MODIS	138.9	28.9	0.11	-110.0	-79.2	124.1	N/A	N/A	N/A	N/A	N/A
CWP (g m ⁻²)		162.2	54.6	0.65	-107.6	-66.3	113.8	N/A	N/A	N/A	N/A	N/A
COT		14.2	2.3	0.73	-11.9	-83.6	12.2	N/A	N/A	N/A	N/A	N/A

*outputs of AOD, CF, CDNC, CWP, and COT are not available from WRF-only simulations

Table 3. The 5-year average performance statistics for chemical variables between two-way WRF-CMAQ and offline CMAQ simulations in winter, 2008-2012.

Variables	Datasets	Mean Obs	Two-way WRF-CMAQ					Offline CMAQ				
			Mean Sim	R	MB	NMB (%)	NME (%)	Mean Sim	R	MB	NMB (%)	NME (%)
Max 8-hr O ₃ (ppb)	AQS	32.4	39.6	0.61	7.2	22.5	23.0	42.3	0.65	9.9	30.7	30.9
	CASTNET	34.9	36.6	0.76	1.7	4.9	9.4	39.7	0.75	4.7	13.5	14.3
PM _{2.5} (μg m ⁻³)	CSN	11.4	10.6	0.21	-0.8	-7.2	29.3	11.7	0.2	0.21	1.8	31.0
	IMPROVE	3.59	3.90	0.83	0.31	8.6	30.3	4.44	0.86	0.85	23.7	32.1
PM ₁₀ (μg m ⁻³)	AQS	19.9	12.7	0.04	-7.2	-36.3	46.9	15.7	0.17	-4.2	-21.3	42.8
	CSN	2.06	1.06	0.78	-1.0	-48.3	48.4	1.02	0.78	-1.04	-50.7	50.8
SO ₄ ²⁻ (μg m ⁻³)	IMPROVE	0.79	0.49	0.95	-0.3	-37.4	38.9	0.49	0.95	-0.3	-38.5	39.9
	CSN	2.37	2.36	0.79	-0.01	-0.3	25.8	2.89	0.81	0.52	21.7	37.8
NO ₃ ⁻ (μg m ⁻³)	IMPROVE	0.73	0.83	0.87	0.1	13.3	40.9	1.06	0.90	0.33	44.6	54.4
	CSN	1.30	0.92	0.80	-0.38	-29.4	30.5	1.03	0.81	-0.27	-21.0	24.1
NH ₄ ⁺ (μg m ⁻³)	CSN	0.69	0.75	0.18	0.06	8.7	58.5	0.79	0.24	0.1	14.2	58.0
	IMPROVE	0.17	0.23	0.80	0.06	40.8	59.2	0.25	0.84	0.09	53.4	65.6
EC (μg m ⁻³)	IMPROVE	0.65	0.74	0.65	0.09	13.0	55.7	0.8	0.67	0.15	23.1	56.4
	CSN	3.05	3.27	0.01	0.22	7.2	53.2	3.49	0.0	0.44	14.4	55.8
TC (μg m ⁻³)	IMPROVE	0.53	0.62	0.75	0.09	17.5	51.3	0.68	0.78	0.15	28.1	52.6
	CSN	1.96	1.56	0.70	-0.4	-20.5	21.6	1.57	0.69	-0.39	-19.8	21.1
Col. CO (10 ¹⁸ mole. cm ⁻³)	MOPITT	26.4	27.6	0.78	1.2	4.7	14.0	28.0	0.19	1.6	5.9	14.3
TOR (DU)	OMI	1.55	1.55	0.86	0.04	0.3	33.5	1.53	0.87	-0.02	-1.2	33.1
Col. NO ₂ (10 ¹⁵ mole. cm ⁻³)	SCIAMACHY	4.87	2.48	0.29	-2.39	-49.0	50.1	2.53	0.28	-2.34	-48.0	49.2
Col. HCHO (10 ¹⁵ mole. cm ⁻³)	SCIAMACHY											

Table 4. The 5-year average performance statistics for chemical variables between two-way WRF-CMAQ and offline CMAQ simulations in summer, 2008-2012.

Variables	Datasets	Mean Obs	Two-way WRF-CMAQ					Offline CMAQ				
			Mean Sim	R	MB	NMB (%)	NME (%)	Mean Sim	R	MB	NMB (%)	NME (%)
Max 8-hr O ₃ (ppb)	AQS	47.9	53.0	0.66	5.1	10.6	13.2	54.8	0.66	6.8	14.2	15.6
	CASTNET	47.2	45.8	0.66	-1.4	-3.0	11.5	47.3	0.68	0.1	0.2	10.5
PM _{2.5} (µg m ⁻³)	CSN	11.4	9.9	0.74	-1.5	-13.2	20.5	9.8	0.71	-1.6	-14.0	20.8
	IMPROVE	6.19	4.52	0.88	-1.66	-26.9	31.2	4.78	0.86	-1.41	-22.8	28.9
PM ₁₀ (µg m ⁻³)	AQS	26.7	14.5	0.03	-12.2	-45.8	50.7	16.2	0.07	-10.5	-39.4	48.6
	CSN	2.86	2.57	0.91	-0.29	-10.2	15.1	2.34	0.91	-0.52	-18.1	19.5
SO ₄ ²⁻ (µg m ⁻³)	IMPROVE	1.40	1.11	0.98	-0.29	-20.9	21.3	1.08	0.98	-0.31	-22.5	22.6
	CSN	0.49	0.71	0.54	0.22	45.2	70.6	0.77	0.59	0.28	57.2	76.8
NO ₃ ⁻ (µg m ⁻³)	IMPROVE	0.20	0.19	0.6	-0.01	-4.7	71.4	0.22	0.63	0.02	10.3	72.2
	CSN	0.91	0.94	0.86	0.03	3.3	22.4	0.88	0.85	-0.03	-3.6	20.1
EC (µg m ⁻³)	CSN	0.56	0.79	0.56	0.23	41.0	56.3	0.79	0.55	0.23	41.9	55.5
	IMPROVE	0.20	0.24	0.56	0.04	20.4	58.8	0.26	0.52	0.06	27.9	63.0
OC (µg m ⁻³)	IMPROVE	1.37	0.70	0.31	-0.67	-49.2	54.0	0.75	0.28	-0.62	-45.4	52.4
	CSN	2.85	2.17	0.54	-0.67	-23.6	29.3	2.19	0.5	-0.65	-22.9	29.7
TC (µg m ⁻³)	IMPROVE	0.88	0.61	0.56	-0.27	-30.5	47.6	0.66	0.53	-0.23	-25.6	47.6
	CSN	1.82	1.32	0.75	-0.5	-27.8	27.8	1.32	0.54	-0.5	-27.3	27.3
Col. CO (10 ¹⁸ mole. cm ⁻³)	MOPITT	1.82	1.32	0.75	-0.5	-27.8	27.8	1.32	0.54	-0.5	-27.3	27.3
TOR (DU)	OMI	35.0	32.2	0.87	-2.8	-8.0	9.0	32.4	0.85	-2.6	-7.3	8.6
Col. NO ₂ (10 ¹⁵ mole. cm ⁻³)	SCIAMACHY	1.08	0.78	0.81	-0.3	-27.8	38.0	0.78	0.80	-0.3	-27.5	38.1
Col. HCHO (10 ¹⁵ mole. cm ⁻³)	SCIAMACHY	5.81	6.71	0.82	0.9	15.0	22.5	6.82	0.82	1.01	17.4	23.5

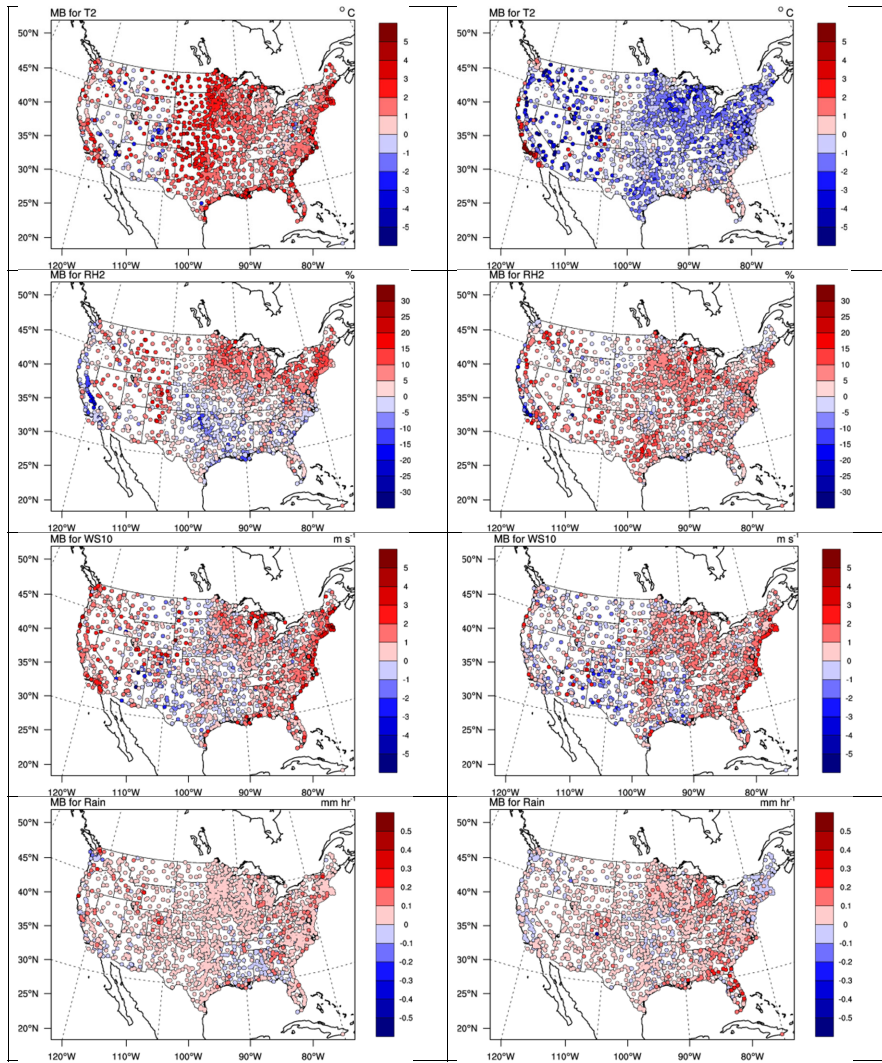
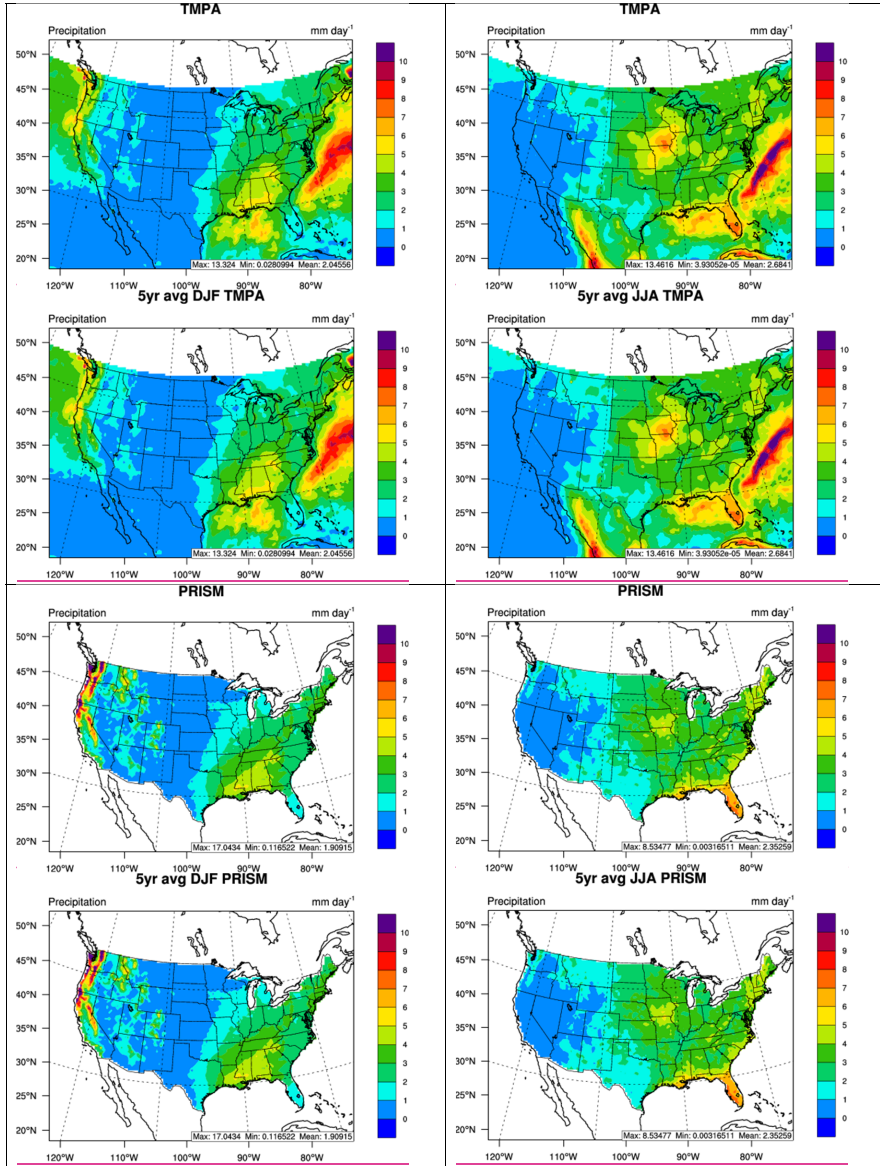


Figure 1. Spatial distributions of 5-year average MBs for 2-m temperature (T2), 2-m relative humidity (RH2), 10-m wind speed (WS10), and hourly precipitation from NCDC for two-way WRF-CMAQ in winter (left panel) and summer (right panel), 2008-2012.



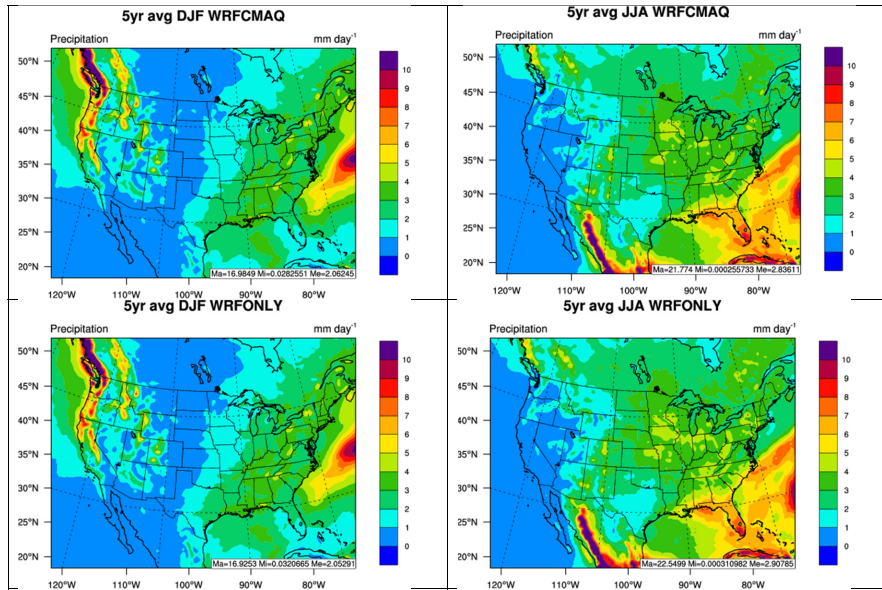


Figure 2. Spatial distributions of 5-year average of daily precipitation from TMPA, PRISM, two-way WRF-CMAQ, and WRF-only (from top to bottom) in winter (left panel) and summer (right panel), 2008-2012.

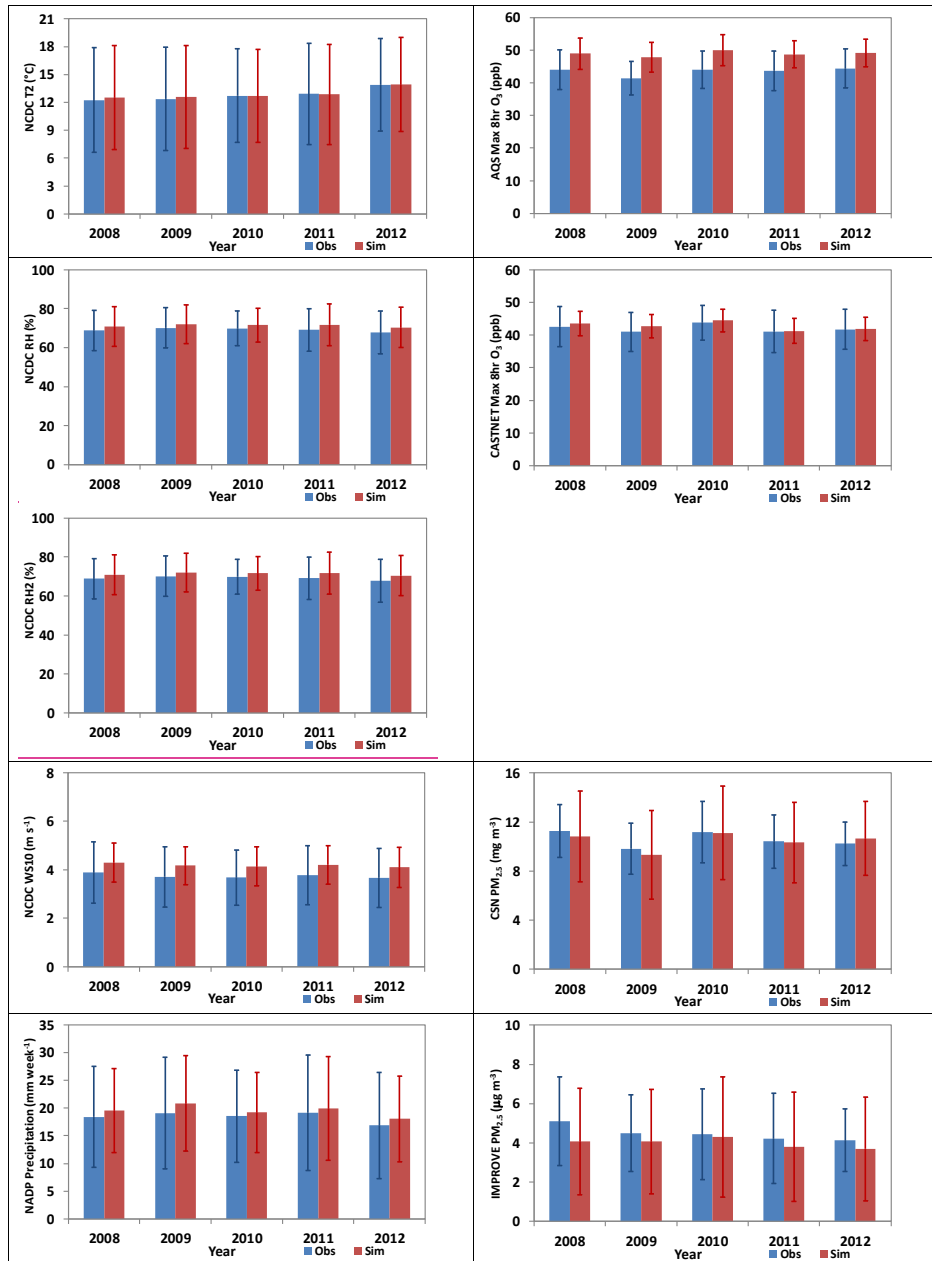
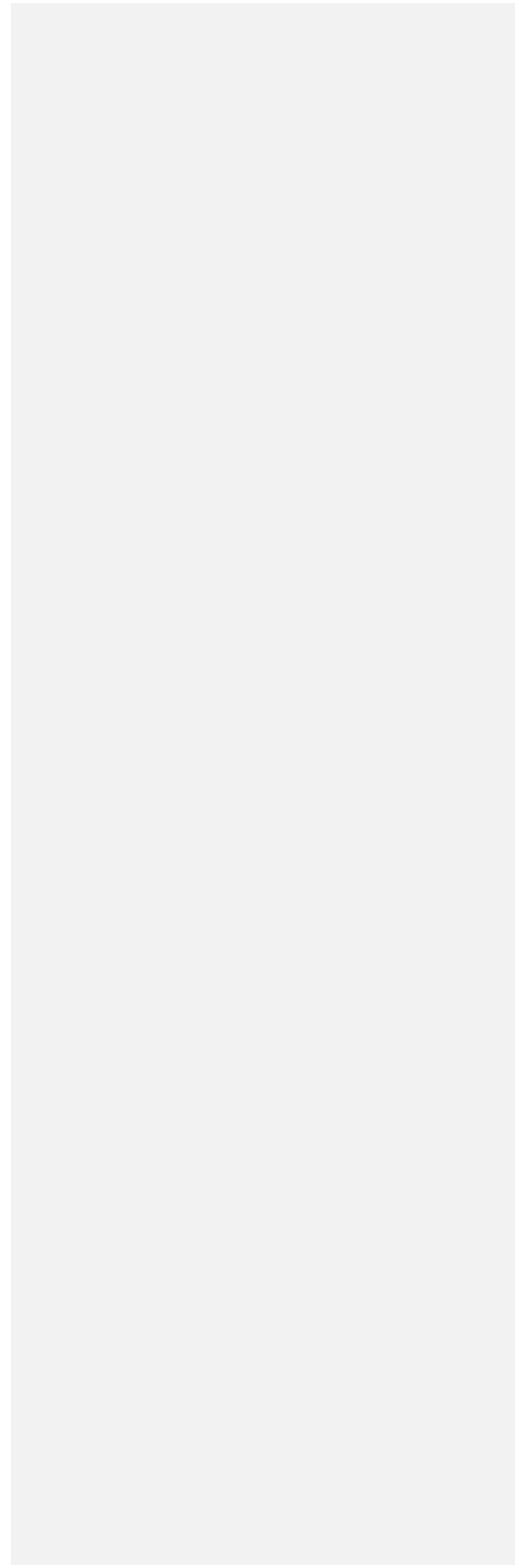
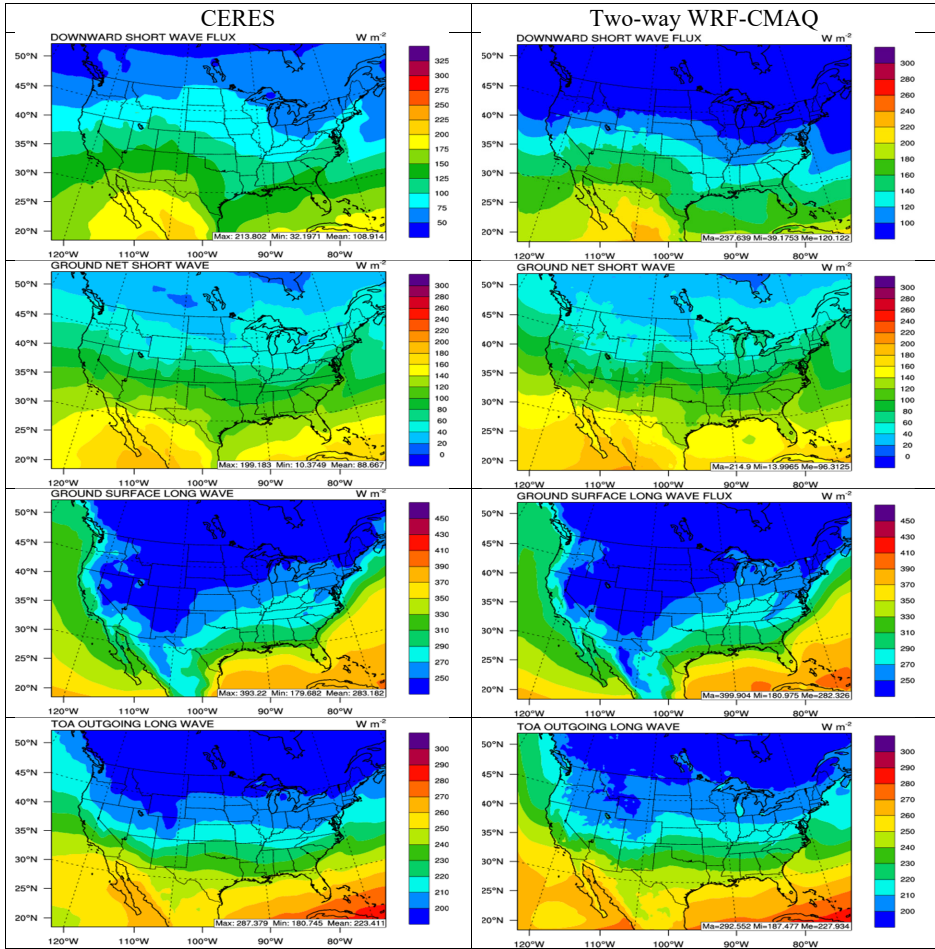


Figure 3. Bar charts for annual average observations and simulations (standard deviations are displayed as the error bars)) from two-way WRF-CMAQ for major meteorological variables (left panel) and chemical species (right panel) in 2008-2012.





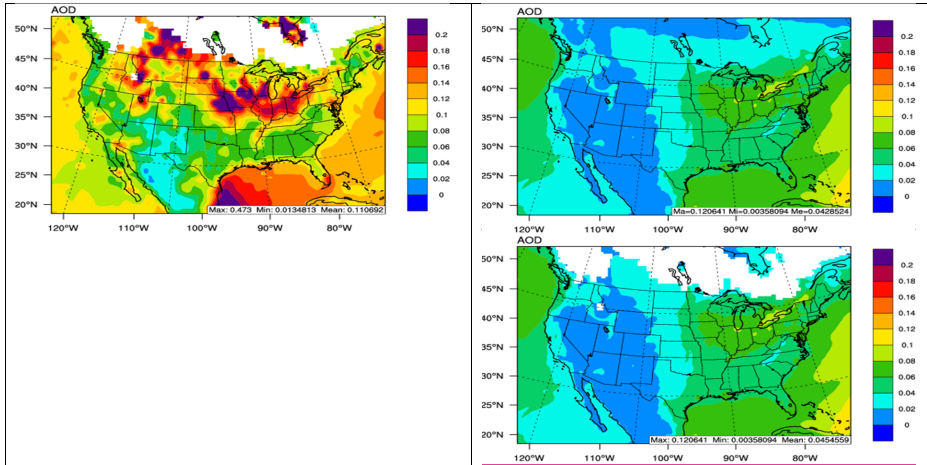


Figure 4. Spatial distribution of 5-year average major radiation variables (from top to bottom: SWDOWN, GSW, GLW, OLR, and AOD) between CERES observations (left panel) vs. two-way WRF-CMAQ (right panel) in winter, 2008-2012.

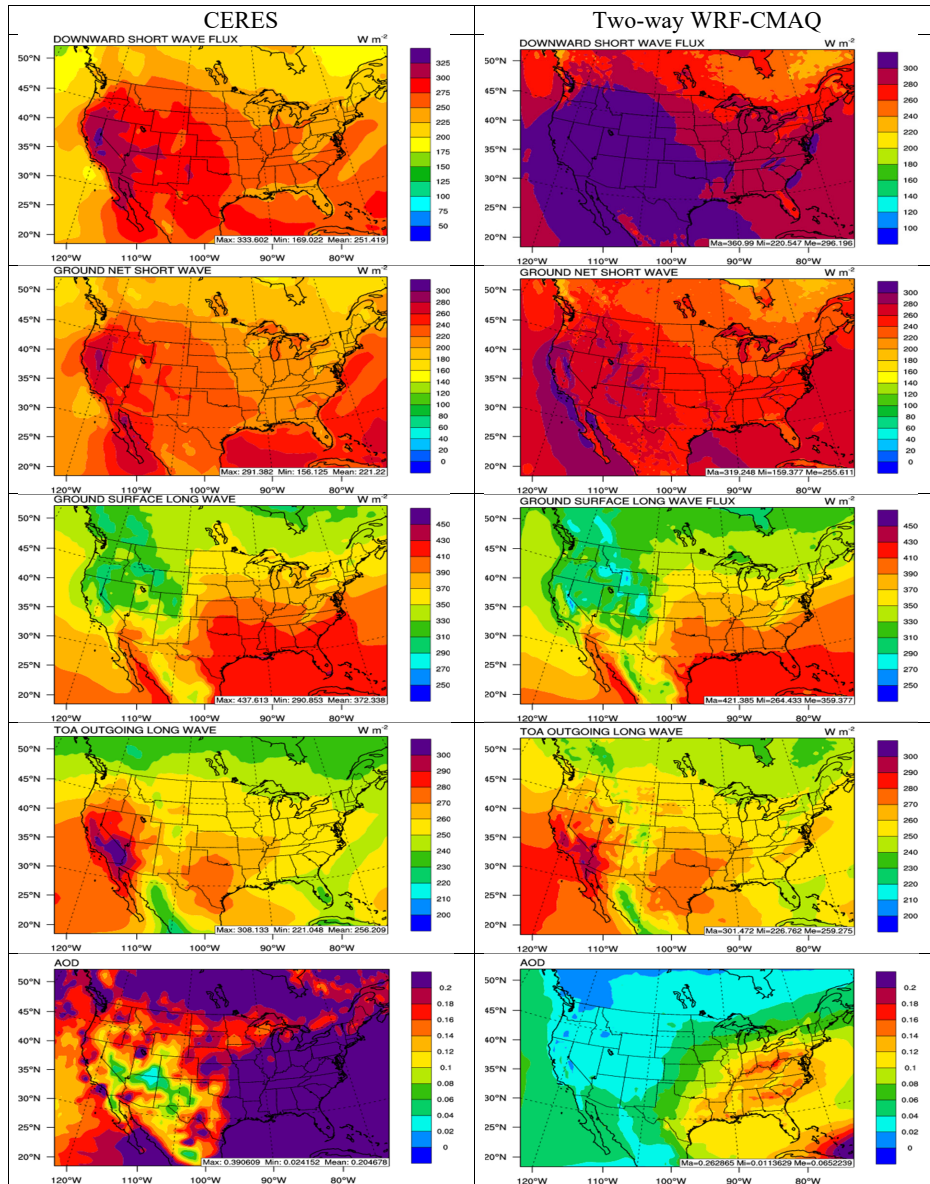
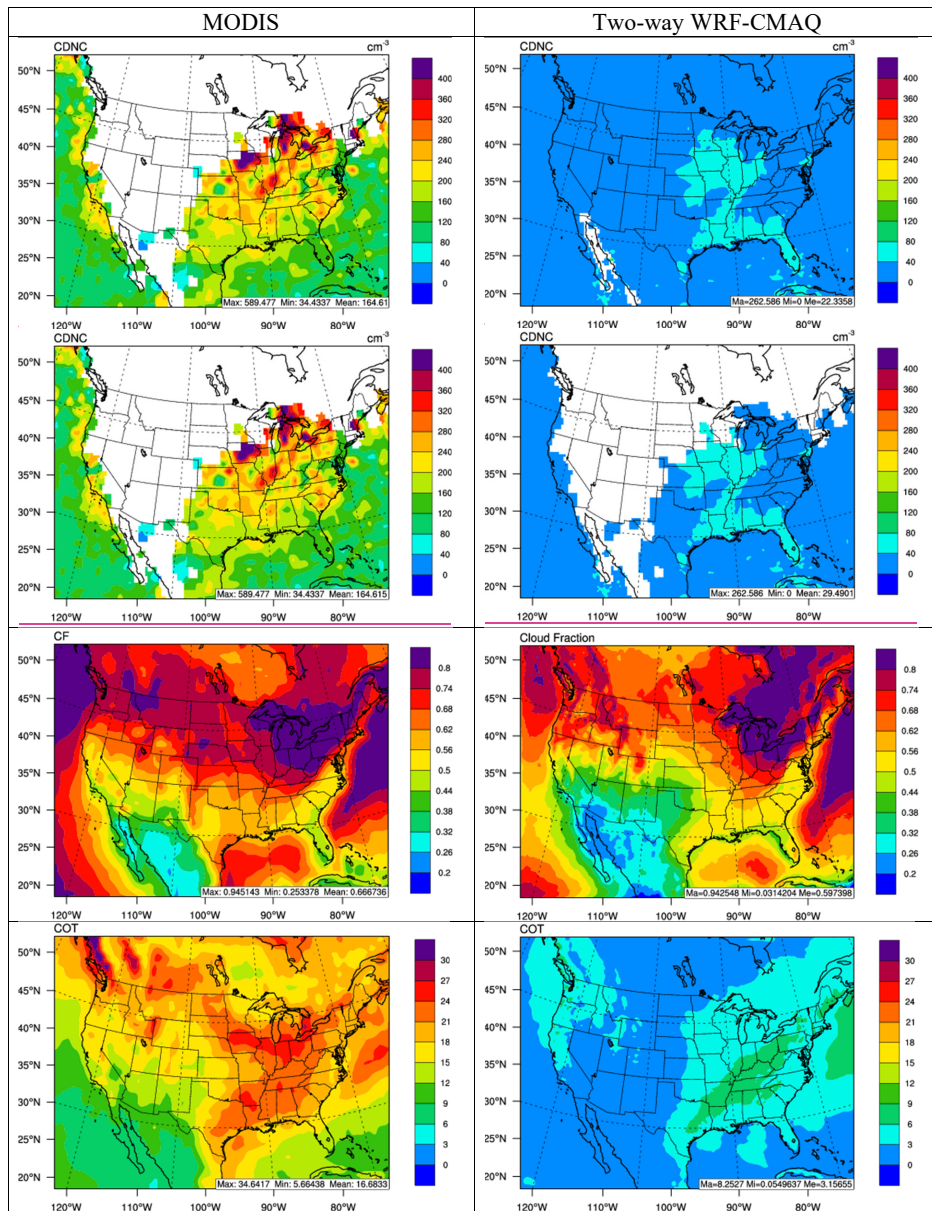


Figure 5. Spatial distribution of 5-year average major radiation variables (from top to bottom: SWDOWN, GSW, GLW, OLR, and AOD) between CERES observations (left panel) vs. two-way WRF-CMAQ (right panel) in summer, 2008-2012.



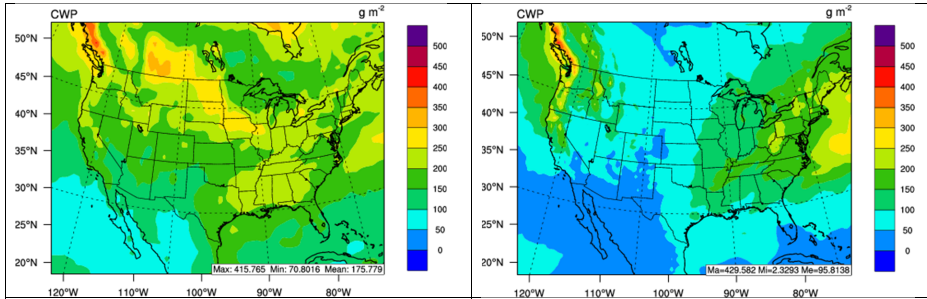
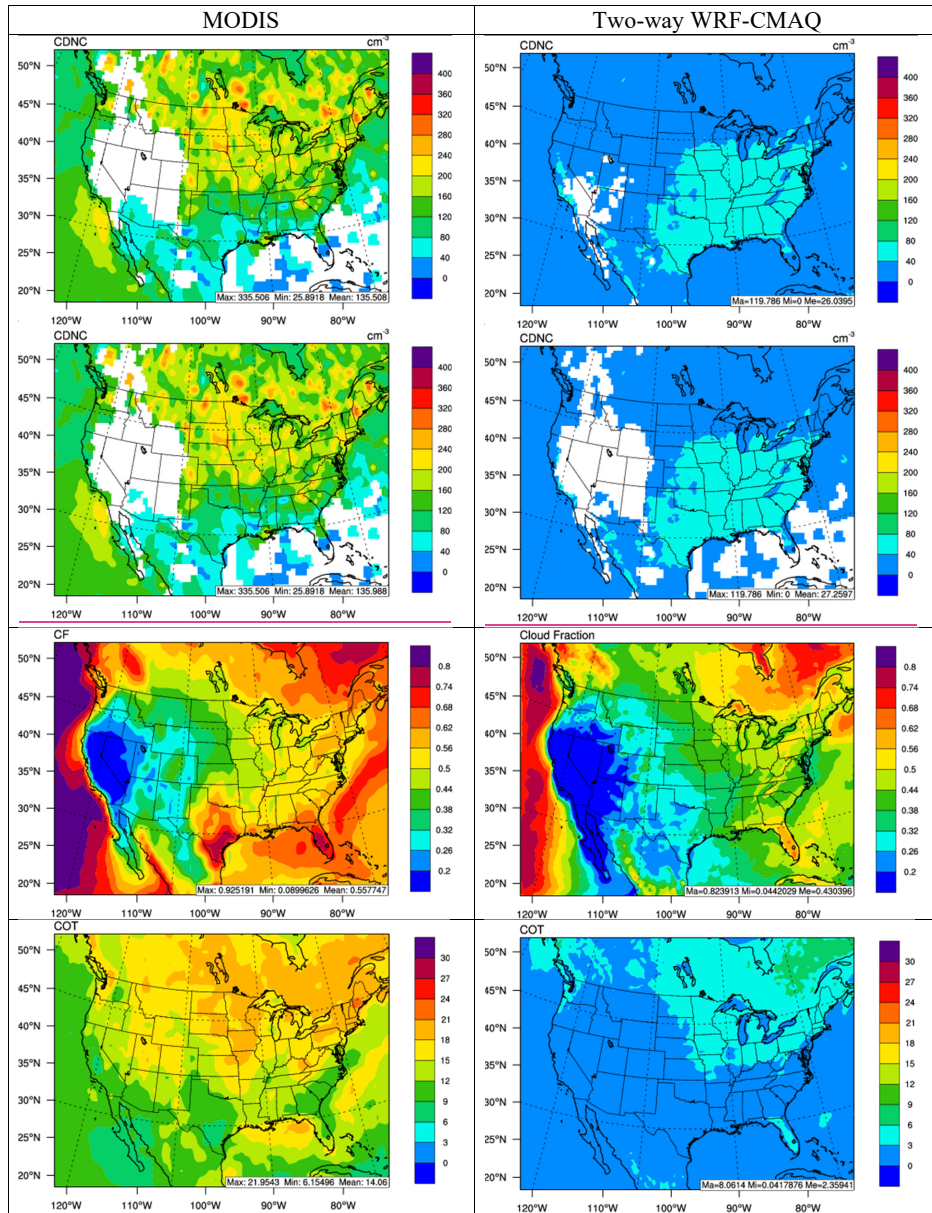


Figure 6. Spatial distribution of 5-year average major cloud variables (from top to bottom: CDNC, CF, COT, and CWP) between MODIS observations (left panel) vs. two-way WRF-CMAQ (right panel) in winter, 2008-2012.



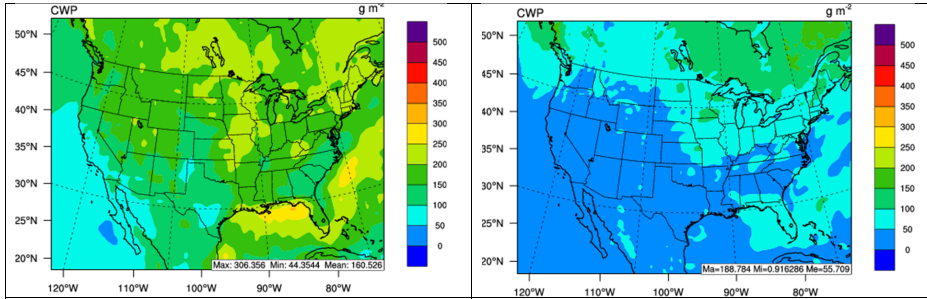


Figure 7. Spatial distribution of 5-year average major cloud variables (from top to bottom: CDNC, CF, COT, and CWP) between MODIS observations (left panel) vs. two-way WRF-CMAQ (right panel) in summer, 2008-2012.

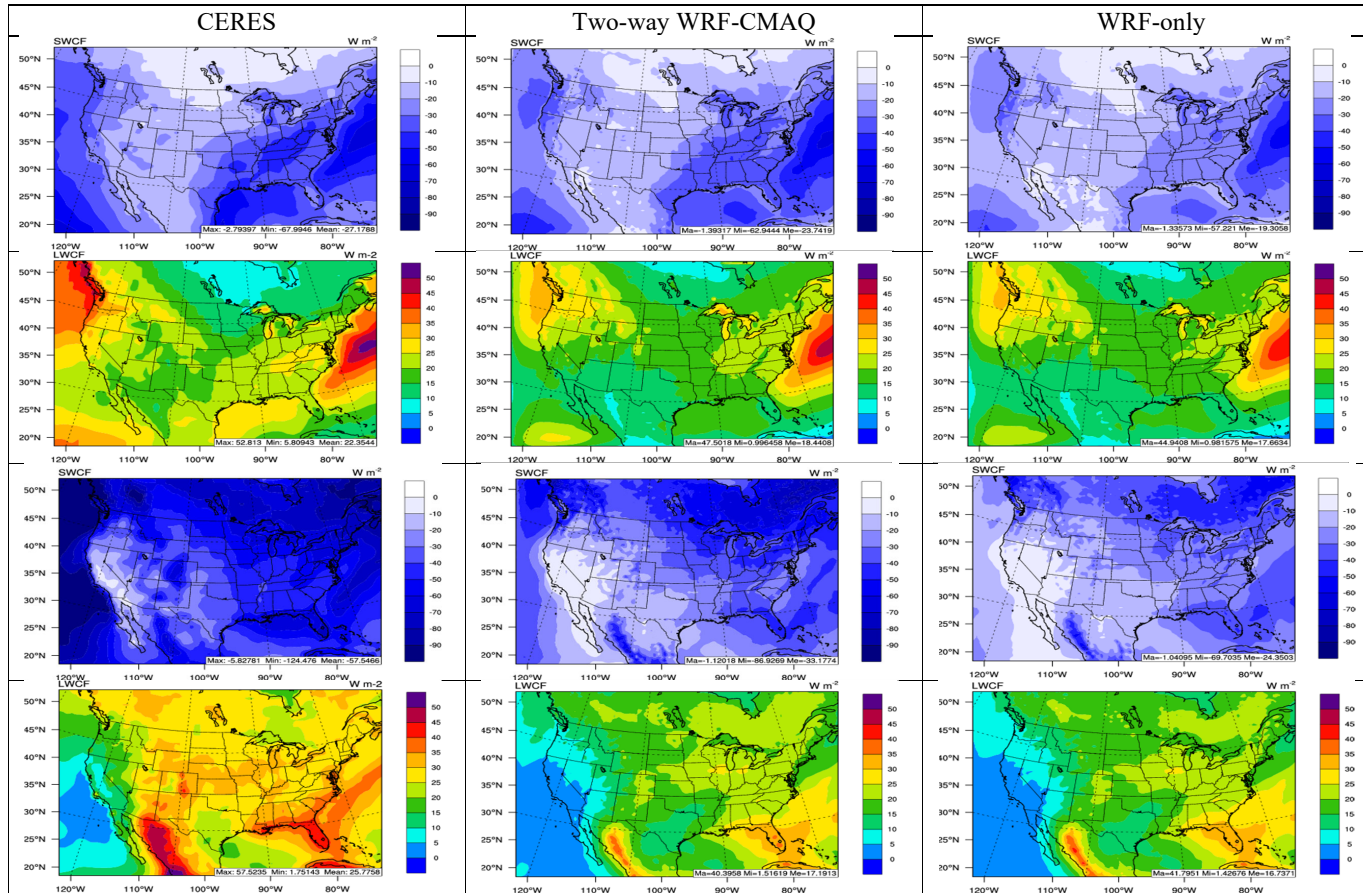


Figure 8. Spatial distribution of 5-year average SWCF in winter, LWCF in winter, SWCF in summer, and LWCF in summer (from top to bottom) between CERES observations (left panel) vs. two-way WRF-CMAQ (center panel) and WRF-only (right panel) in 2008-2012.

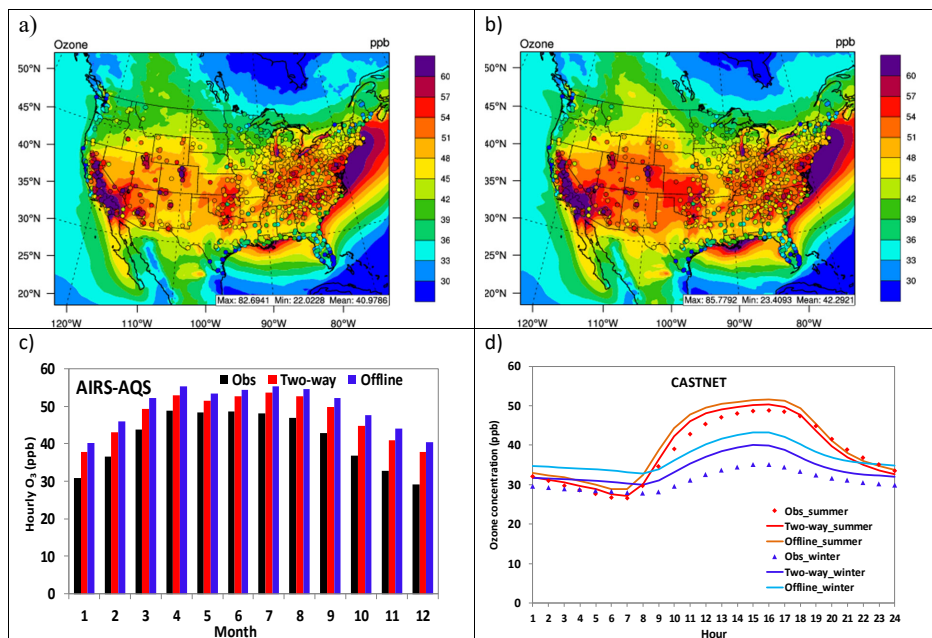


Figure 9. Spatial distributions of 5-year averaged max 8-h O_3 in summer overlaid with observations from AIRS-AQS and CASTNET for a) two-way WRF-CMAQ and b) offline CMAQ; c) bar chart for 5-year average monthly O_3 between observations (black bar), two-way WRF-CMAQ (red bar), and offline CMAQ (blue bar); and d) diurnal plots of observed (dots) vs. simulated (lines) hourly O_3 concentrations against CASTNET for winter (cold colors) and summer (warm colors) in 2008-2012.

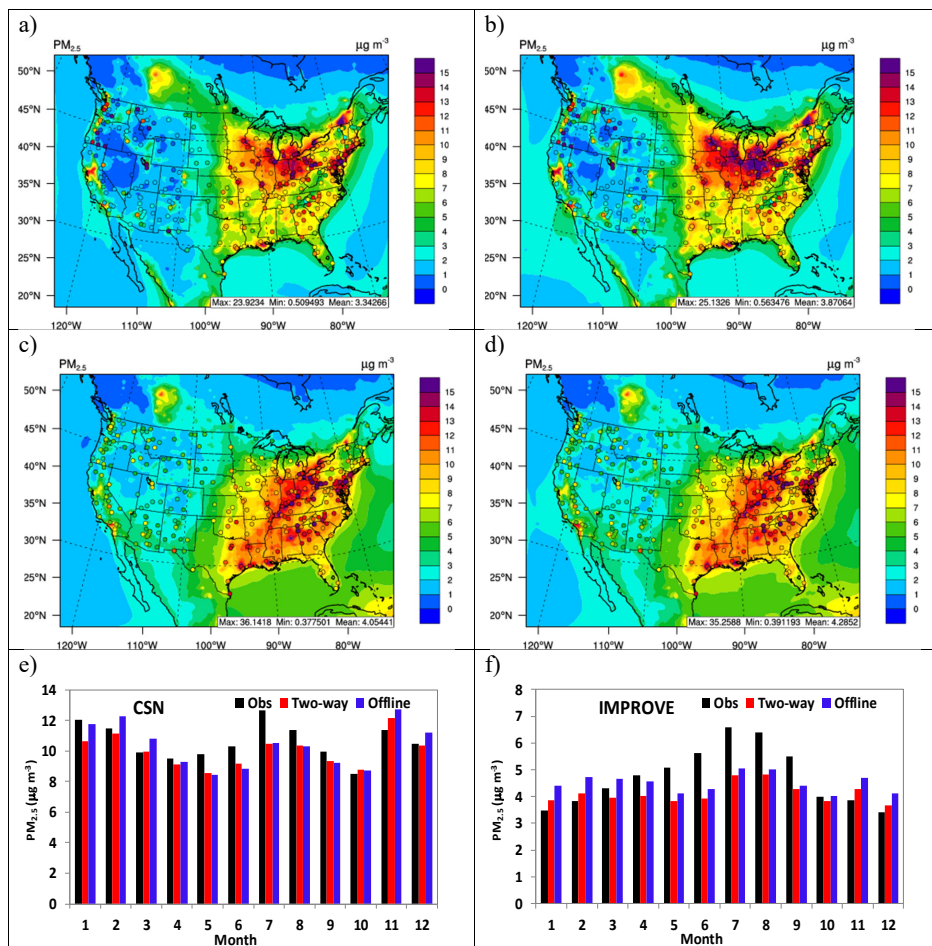


Figure 10. Spatial distributions of 5-year averaged daily PM_{2.5} overlaid with observations from CSN and IMPROVE for two-way WRF-CMAQ in a) winter and c) summer and offline CMAQ in b) winter and d) summer; bar charts for 5-year average monthly PM_{2.5} between observations (black bar), two-way WRF-CMAQ (red bar), and offline CMAQ (blue bar) over e) CSN and f) IMPROVE in 2008-2012.

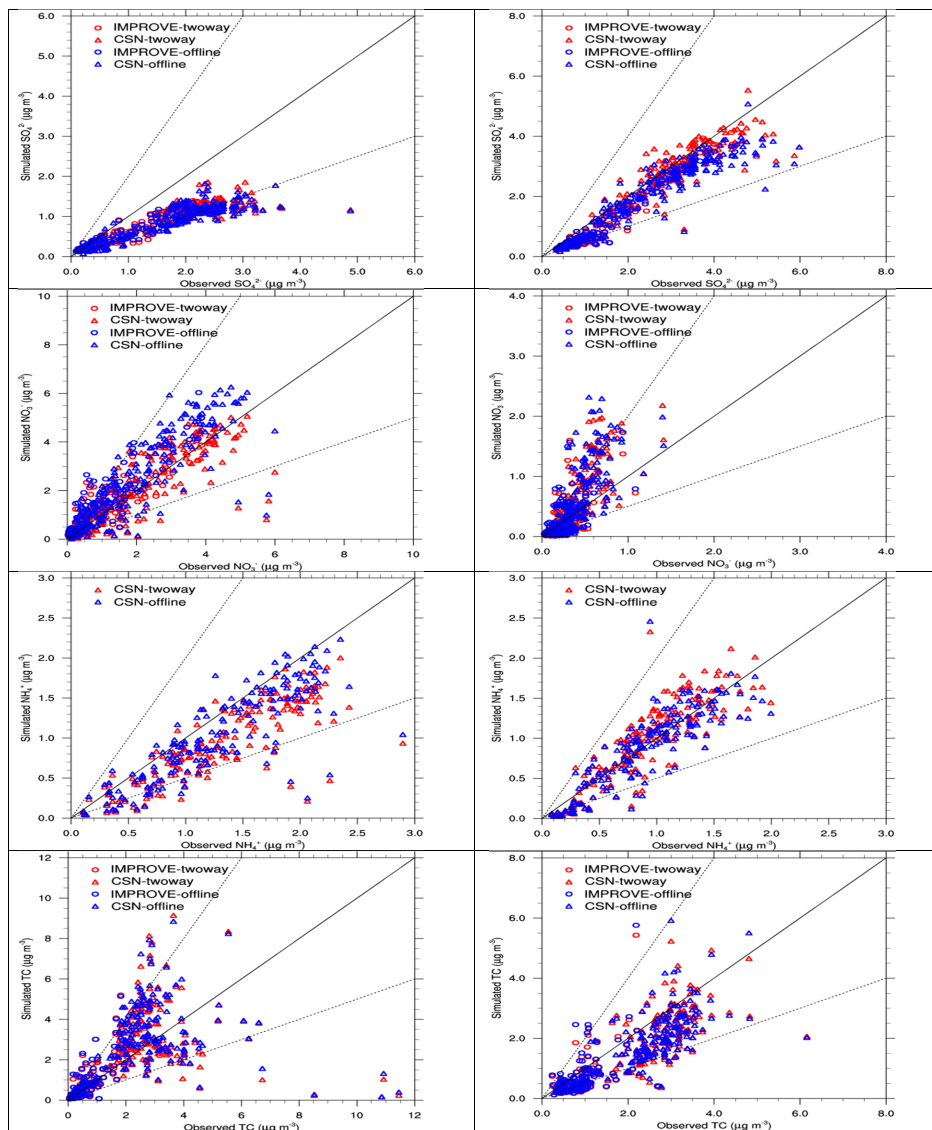
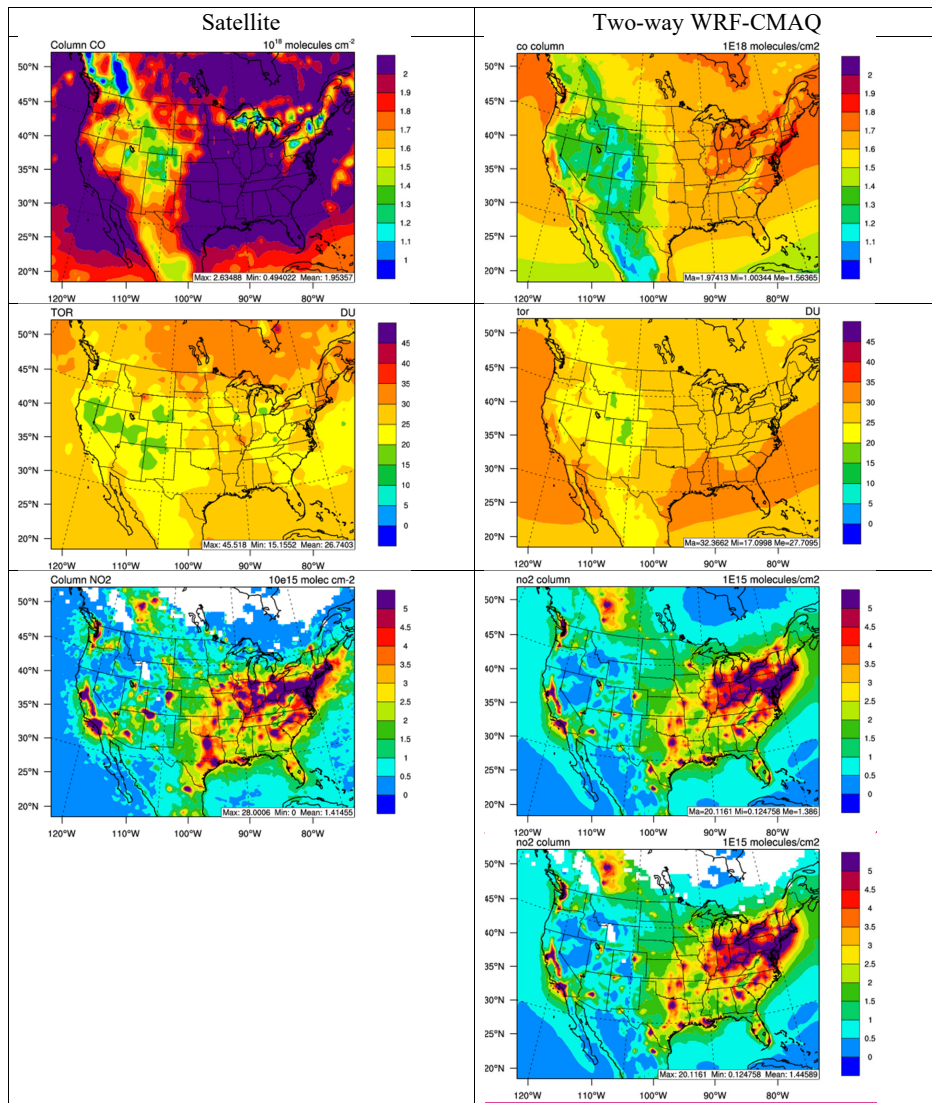


Figure 11. Scatter plots of 5-year averaged PM_{2.5} constituents for SO₄²⁻, NO₃⁻, NH₄⁺, and TC (from top to bottom) between observations and simulations of two-way WRF-CMAQ (red color) and offline CMAQ (blue) in winter (left panel) and summer (right panel), 2008-2012.



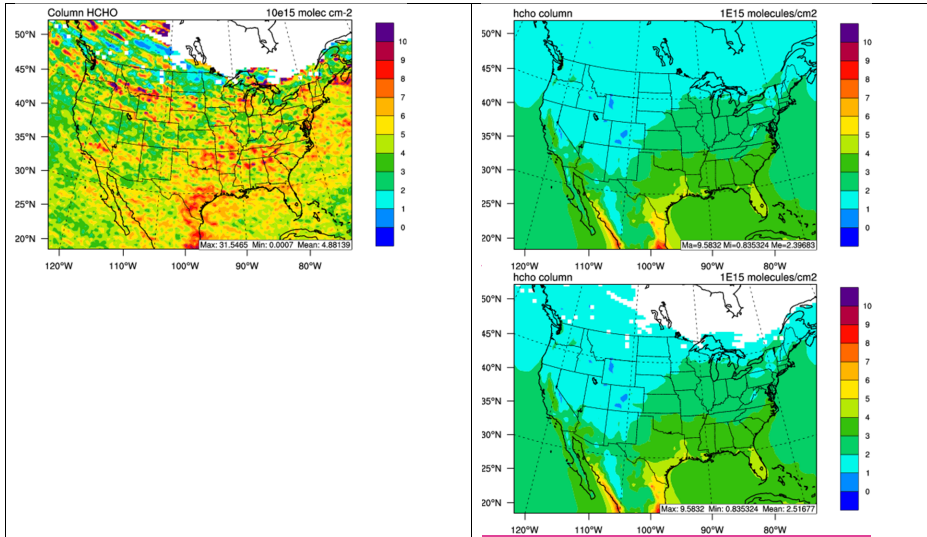


Figure 12. Spatial distribution of 5-year average column abundances (from top to bottom: column CO, TOR, column NO₂, and column HCHO) between various satellite observations (left panel) vs. two-way WRF-CMAQ (right panel) in winter, 2008-2012.

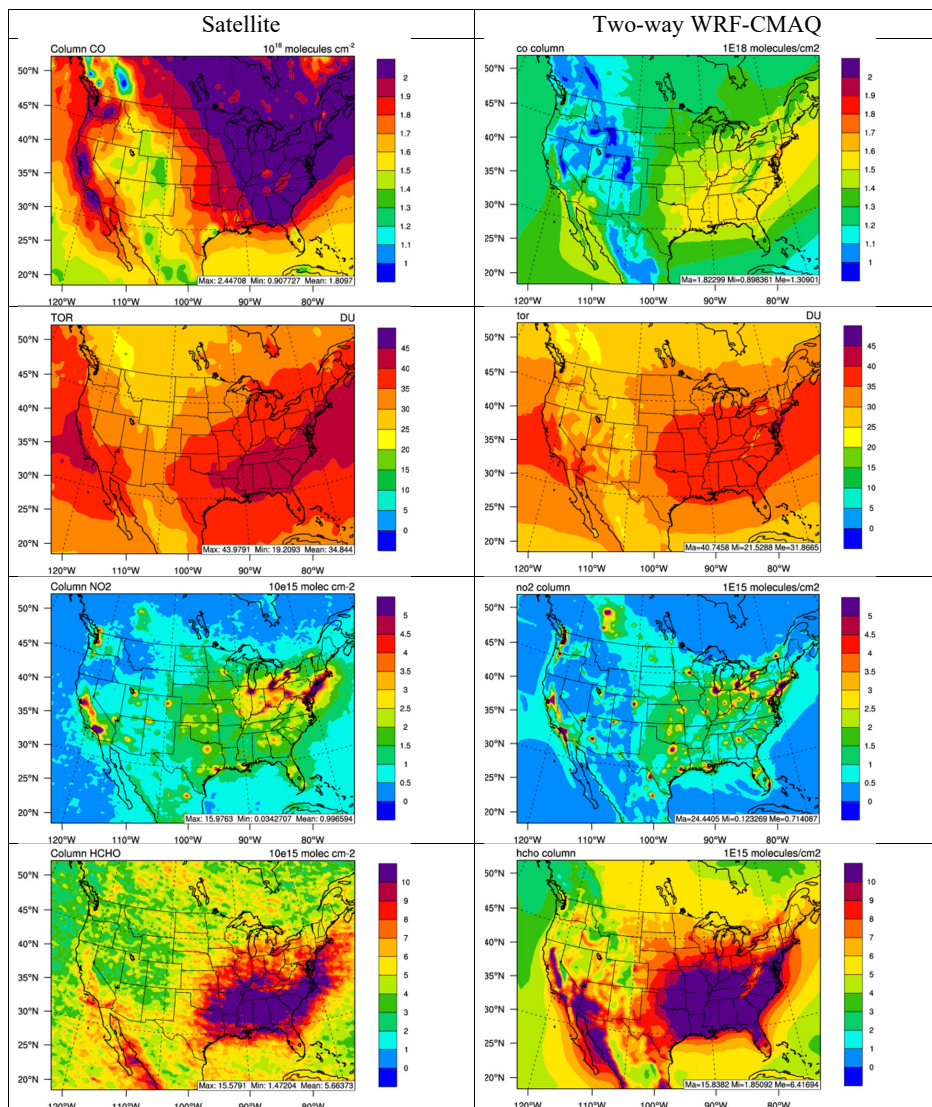


Figure 13. Spatial distribution of 5-year average column abundances (from top to bottom: column CO, TOR, column NO₂, and column HCHO) between various satellite observations (left panel) vs. two-way WRF-CMAQ (right panel) in summer, 2008-2012.

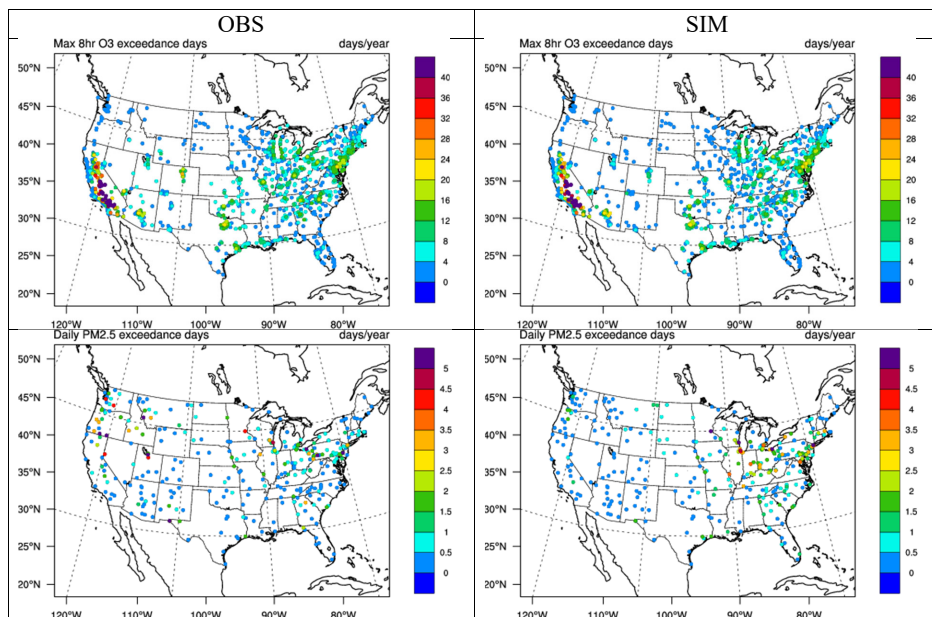


Figure 14. The spatial distribution of 5-year average annual exceedance days of max 8-h O_3 and daily $PM_{2.5}$ between observations (O_3 over the AIRS-AQS/CASTNET network and $PM_{2.5}$ over the IMPROVE/CSN network) and two-way WRF-CMAQ in 2008-2012.

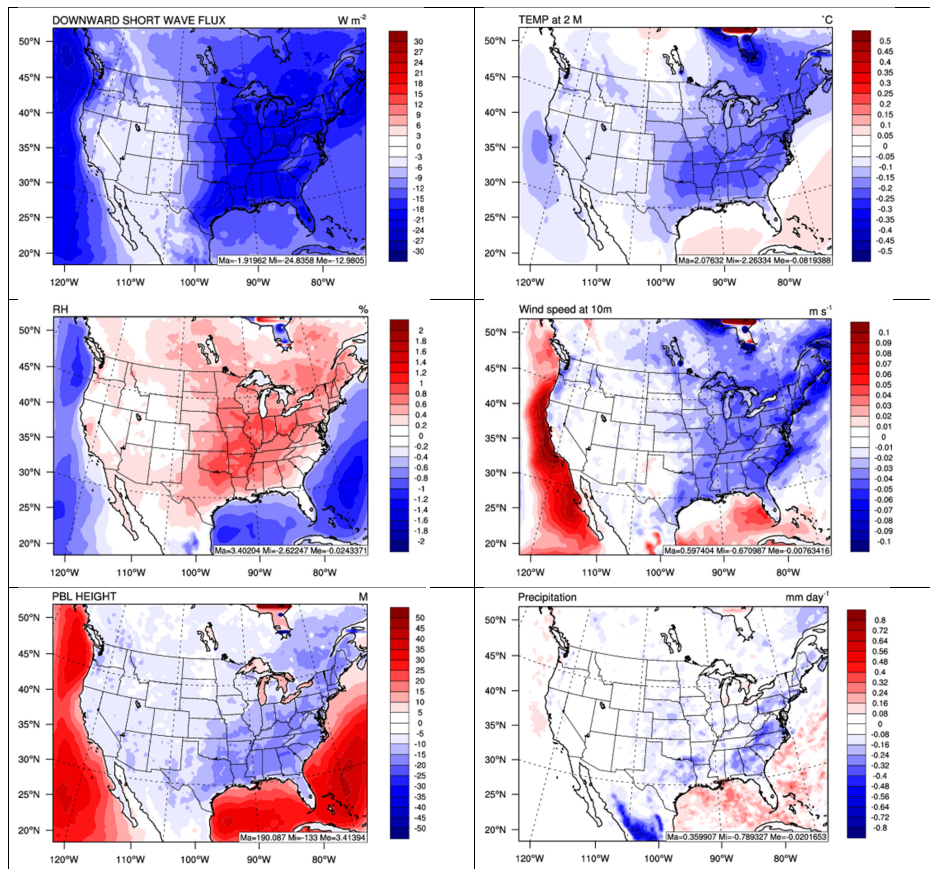


Figure 15. Spatial difference plots (two-way WRF-CMAQ - WRF-only) for major meteorological variables between two-way WRF-CMAQ and WRF-only in 2008-2012.

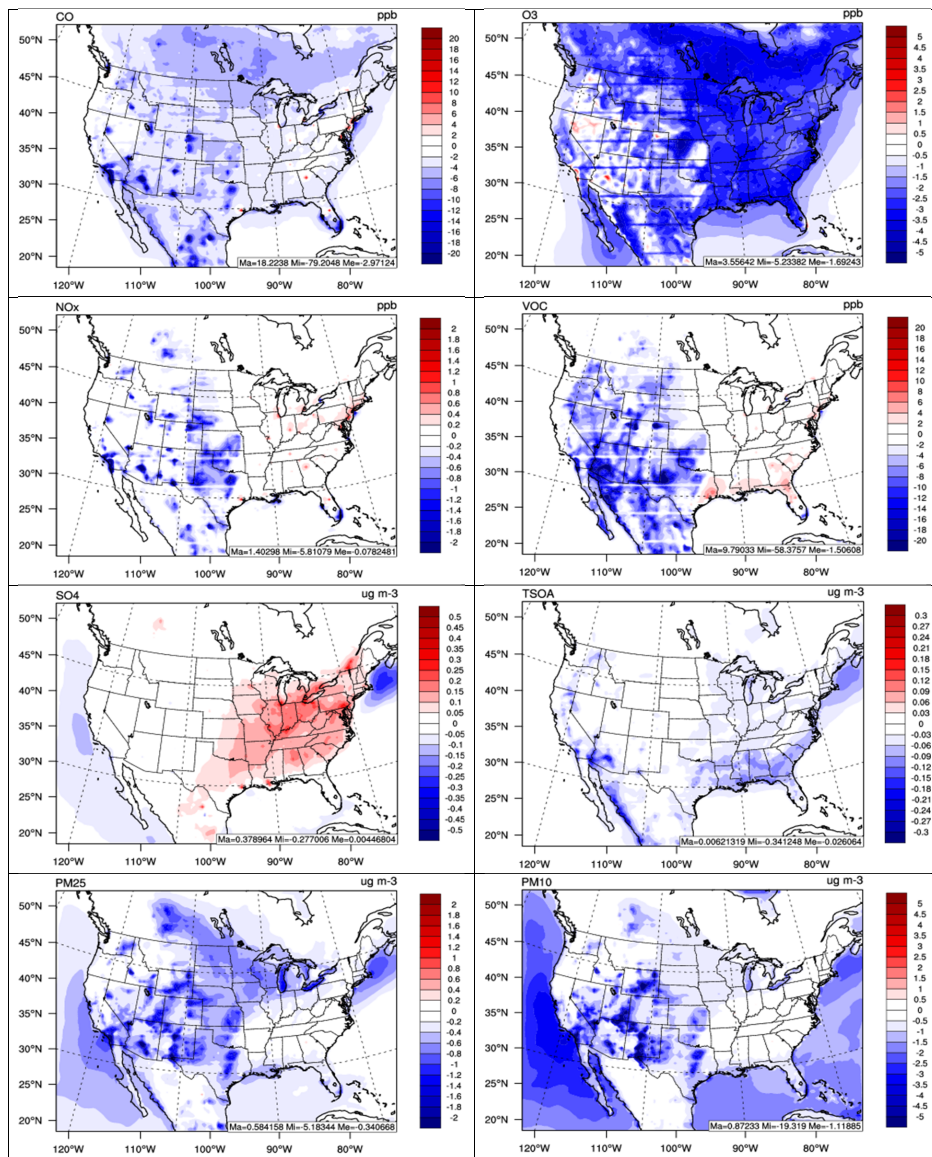


Figure 16. Spatial difference plots (two-way WRF-CMAQ - offline CMAQ) for major chemical species between two-way WRF-CMAQ and offline CMAQ in 2008-2012.